THEORETICAL AND EXPERIMENTAL STUDIES
OF
COMPTON SCATTER DENSITOMETRY

by

Michael Ebipa Ebifegha

A thesis submitted to the Faculty of Graduate Studies in partial fulfillment of the requirements for the degree of Master of Science.

Department of Physics
Carleton University
Ottawa, Ontario

May, 1980

The undersigned recommend to the Faculty of Graduate Studies acceptance of the thesis "Theoretical and Experimental Studies of Compton Scatter Densitometry" submitted by Michael Ebipa Ebifegha, in partial fulfillment of the requirements for the degree of Master of Science.

W. J. Romo for R.L. Clarke

Thesis Supervisor

M. K. Sundaresan

Chairman, Department of Physics

Carleton University

ABSTRACT

The effects of multiple scattering in X-ray Compton scatter densitometry is discussed. A mathematical expression for double scattering intensity is derived. A reduction of about 50% in the observed discrepancy between the Compton density and the Archimedes density is achieved.

A Compton scatter densitometry equation which includes both the incoherent and coherent scattering cross-sections is proposed.

ACKNOWLEDGEMENTS

I express my profound gratitude to our Lord God for His excellent support both physically and spiritually.

I wish to express my sincere thanks to Prof. R.L. Clarke for his supervision. It is a pleasure to acknowledge the advice of Prof.W.J. Romo and K. Hafner; M. Morbey for his library assistance; J. Sliwka for his technical assistance; and R. O'Driscoll for typing this thesis.

Finally, I would like to express my appreciation to Ahmadu Bello University, Zaria, Nigeria for the financial support and Prof. D.E. Ajakaiye for the encouragement.

TABLE OF CONTENTS

LIST OF TABLE

LIST OF FIGURES

DEDICATED TO THE GLORY OF GOD

1 - INTRODUCTION

A knowledge of the body mineral content is of value since it is one of the physical indicators in the clinical investigation of the various disease states. The information on the body mineral content, for example, is valuable in the diagnosis of such diseases as Osteomalacia and Osteoporosis as well as in the continuing study of bone formation, development and removal processes and overall human development [10]. The mineral content of the body usually diminishes after middle age, sometimes to such an extent that the bone strength is seriously reduced. The Physician must therefore have some way of measuring the mineral content if the loss of mineral is to be controlled by diet or drugs. For non-living subjects the measurement of the mineral content is simple and straightforward. For living subjects the determination has to be done in-vivo and therefore requires special techniques.

For several years the quantitative determination of bone mineral content has constituted one of the research areas in medical physics. However, due to the complicated nature of the problem with the consequential limitations needed to uphold the safety of the patient, different versions of bone mineral content determination in vivo have emerged in the past decade.

There are at present two major clinical methods for in vivo measurement of bone mineral content. These are the Radiographic technique which makes use of an X-ray source and a standard (aluminum wedge) and Photon absorptiometry technique which uses a radio-isotope and a scintillation detector.

In the Radiographic technique [11, 21, 23, 29], the exposure images of the standard wedge and the bone under investigation are obtained simultaneously on film. The X-ray attenuation through the investigated bone and the wedge are compared by means of a photo-densitometer and computer. To relate the attenuation to a density the assumption is made that attenuation in the skin and flesh is small and that the bone being investigated has a known shape. Then from the volume of the bone section and the attenuation in passing through that section, it is possible to determine the relative amounts of the various constituents from knowledge of the chemical composition of the bone. Extensive research work has been carried out on this technique [29]. Precision of better than 20% is difficult to obtain with this technique and this makes it not quite satisfactory for practical use in clinics where high accuracy is desired.

In the photon absorptiometry technique developed by Cameron and Sorenson [2], a well collimated beam of photons supplied by a radioactive source, usually Iodine-125 at 27.3 keV or Amercium-241 at 59.6 keV is scanned across the bone under investigation, and the transmitted beam is then detected with a conventional scintillation detector. The scan measures the count rate relative to the rate with no sample present. The total absorption is then obtained from the area under the curve of counts below the no sample level as a function of position across the bone. By assuming a composition for the bone and determining the volume of the bone from the width of the bone as indicated by the scan, a mineral content per unit length is determined.

A method of bone mineral analysis using computed tomography has recently been developed by the Department of Biomedical Engineering, Swiss Federal Institute of Technology and University of Zurich [14]. In this technique [14] the subject is scanned transaxially at a selected site with a narrow beam of gamma and X-rays from a radionuclide. The intensity of the transmitted beam is measured at intervals, and the linear translation movement of source and detector(s) is repeated at different angles. The distribution of the linear attenuation coefficient is calculated from the measured transmission data. The resulting matrix of over 16,000 local linear attenuation coefficients is visualized in the form of a cross-sectional (density) image [14]. Although this system is highly sensitive with a high precision scanning unit and reliable microcomputer unit [14], it may probably be very expensive. The use of the ratio of the peak area of the coherently scattered photon and the Compton scattered photon in the determination of the density of a substance has been developed by Olkkonen et al [22]. The measuring procedure consists of the detection of the scattered photons in a narrow beam geometry using a semi-conductor detector and a multichannel analyzer. The fine energy resolution of the system separates the peaks due to the coherently and Compton scattered photons in the scattering spectrum. The difference in the attenuation of the coherently and Compton scattered photons however constitutes the principal error in this method [22].

In the techniques described above there is the disadvantage that either some assumption has to be made about the shape of the bone and its chemical composition or the measuring system may be highly expensive.

A method for determining the electron and physical density in bone tissue which does not require a prior knowledge of the shape of the bone and the surrounding tissue has been developed by Clarke and Van Dyk [6] and also by Kennett and Webber (18,27). The method requires the measurement of the ratio of Compton scattered to unscattered gamma rays as a beam of collimated gamma rays passes through the region under investigation. The problems of expense, availability, simplicity and long exposure times encountered when a radioactive source is used prompted the need for a continuous source of X-rays (21,29). The present system uses a conventional medical X-ray machine as the source of photons. It has the advantage of permitting measurement of bones of different sizes and shapes without recalibration and requires no detailed knowledge of the surrounding material [21,29]. However, the practical achievement of these advantages have been grossly limited by the assumptions invoked in the theoretical derivation of the technique [6,18, 27]. The theory did not take into account effects such as multiple scattering, coherent scattering and geometric effects. The elimination of these side effects from the measured density has attracted the attention of several researchers [13, 15, 18, 21, 27, 29].

The work presented here is part of such efforts to achieve a balance between theory and practice. We shall proceed by first studying the theory of Compton scattering densitometry. This will be followed by a description of the current X-ray Compton scatter densitometer developed in the Department of Physics, Carleton University. We shall discuss the flaws caused by multiple scattering in the results obtained with the Compton densitometer and proceed further to derive a mathematical correction term. This will be followed by a discussion of the effects due to coherent scattering. A description of the measurement procedure will be followed by actual experimental measurements taken with the Compton densitometer. The correction factor for multiple scattering will then be applied to the observed results. The final result after correcting for multiple scattering will then be compared with standard values.

2 THEORY OF COMPTON SCATTER DENSITOMETRY

The theory of Compton scatter densitometry is discussed in detail by Clarke and Van Dyk (6), Mortimer (21) and White (29). The present study uses the low energy method.

The scattered radiation under consideration arises from Compton interactions. In Compton scattering the interaction takes place with a loosely bound electron, resulting in an energy loss in the scattered photon. The energy $E_1 = h\nu$ of the incident photon and the energy $E_2 = h\nu^1$ of the scattered photon in a Compton interaction are related to the angle of scattering by the following relation [9]

$$P = \frac{E_2}{E_1} = [1+\alpha(1-\cos\theta)]^{-1} \qquad (2\text{-}1)$$

where $\alpha = E_1/mc^2$ is the initial photon energy in electron rest mass units.

For low energy photons ($\alpha << 1$) the change in energy due to Compton scattering is negligible so that θ can be determined from geometric consideration [6].

The configuration of sources and detectors for the measurement of electron density discussed in this text was designed by Kapoor [15]. In this configuration (fig.2-1) three collimated detectors D_1,D_2 and D_3 and a single source of photons are used. The sensitive volume marked X is defined by the projected intersection of the detector and source collimators. The detectors are equidistant from the sensitive volume.

If the average intensity of the source is I_o photons per second and the energy is E_o, the transmitted and scattered intensities detected in the source position 1 are respectively given by

$$T_1 = I_o A_{ox} A_{x3} E_3 \qquad (2\text{-}2)$$

$$S_1 = I_o A_{o\bar{x}} B_{x1} E_1 G$$

where A_{ox} and A_{x3} are the transmission factors of the beam of energy E_o along the paths ox and x3; and B_{x1} is the transmission factor for the scattered beam along path x1

E_1 and E_3 are the efficiences of detectors D_1 and D_3 respectively.

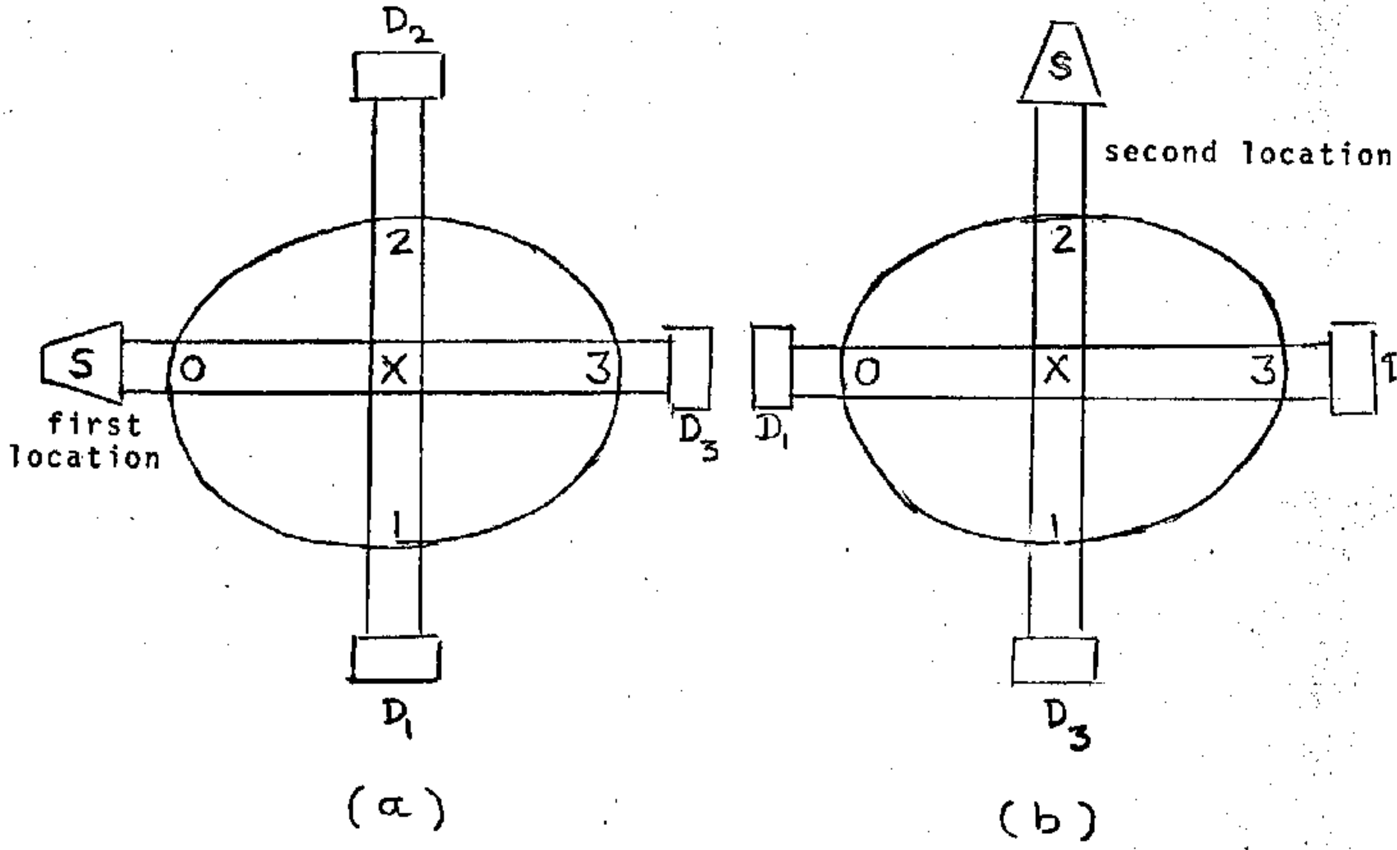

Fig.2-1: Configuration of Source and Detectors for Electron Density Measurement Using the Low-Energy Technique [15]
(a) Initial Configuration; (b) Source Moved to Second Location

G is a factor made up of the Compton cross-section for E_0 scattered through angle θ_1 and the number of electrons per cm^3 of the selected volume (i.e. the electron density).

From equation (2-2) we obtain

$$\frac{S_1}{T_1} = \frac{B_{x1}\, E_1\, G}{A_{x3}\, E_3} \qquad (2\text{-}3)$$

Similarly the ratio of the scattered (S_2) to the transmitted (T_2) beams for the source position 2 will be given by

$$\frac{S_2}{T_2} = \frac{B_{x3}\, E_2\, G}{A_{x1}\, E_3} \qquad (2\text{-}4)$$

From equations (2-3) and (2-4) we have

$$\frac{S_1}{T_1}\frac{S_2}{T_2} = \frac{B_{x1}\, B_{x3}\, E_1 E_2\, G^2}{A_{x1}\, A_{x3}\, E_3^2} \qquad (2\text{-}5)$$

Equation (2-5) can be simplified by assuming that the attenuation of the scattered and transmitted beams are the same, that is,

$B_{x1} = A_{x1}$ and $B_{x3} = A_{x3}$

The density dependent factor is then given by

$$G = \frac{E_3}{\sqrt{E_1E_2}}\left(S_1S_2/T_1T_2\right)^{1/2} = K\left(S_1S_2/T_1T_2\right)^{1/2}$$

The constant k is determined by conventional calibration techniques. S_1, S_2, T_1 and T_2 are the observed counting rates.

CALIBRATION

The apparatus dependent factors entering into G can all be found empirically or calculated [6]. However if the electron density $(\rho_e)x$ of an unknown sample is measured relative to the electron density $(\rho_e)s$ of a standard sample (e.g. water or lucite) the apparatus dependent factors cancel out so that the ratio R_e is ;

$$R_e = \frac{G_x}{G_s} = \frac{(\rho_e)x}{(\rho_e)s} = \frac{\left(S_1S_2/T_1T_2\right)_x^{1/2}}{\left(S_1S_2/T_1T_2\right)_s^{1/2}} \qquad (2\text{-}6)$$

Where the subscripts x and s refer to the unknown and standard samples respectively.

EVALUATION OF PHYSICAL DENSITY

(1) The relative electron density R_e and the physical densities ρ_x and ρ_s of the unknown and standard materials respectively may be related to the chemical composition of the materials by the relation [6].

$$R_e = \left[\frac{\sum_i Z_i a_i}{\sum_i A_i a_i}\right]_x \left[\frac{\sum_i Z_i a_i}{\sum_i A_i a_i}\right]_s^{-1} \frac{\rho_x}{\rho_s} \qquad (2-7)$$

where Z_i and A_i are the atomic number and atomic weight of the i^{th} constituent

a_i is the number of atoms of the i^{th} element per molecule and the sum is over all elements in the compound.

Equation (2-7) is based on the assumption that the number of electrons per unit volume is constant [6].

In deriving equations (2-6) and (2-7) it was assumed that the attenuation of the scattered and transmitted beams are the same when each traverses the same path. The theory also assumes that geometric effects, coherent and multiple scattering effects are negligible. Experiments [13, 15, 18, 21, 27, 29], however have shown that these quantities have measureable effects for some photon energies.

3 EXPERIMENTAL APPARATUS

The measurement system was designed in stages by Mortimer [21], White [29] and Kapoor [15]. It consisted essentially of an X-ray source, a system for positioning the object of interest within the sensitive region defined by the Collimator's geometry, three photon detectors and the associated electronics. (figs, 3-1, - 3-3).

The X-ray source was a Picker portable unit capable of producing 90 kv rms at a maximum current of 15 ma. This unit made use of a half-wave rectified voltage supply. The head of the X-ray generator was designed so that it could be rotated through 90^{o} from some position 1 to some other position 2 (fig. 3-1). The scattered X-rays were detected by two NaI(Tℓ) crystal scintillators and the transmitted beam was detected by a CsI(Na) crystal scintillator. The crystal scintillators were optically coupled to photo multiplier tubes. The scintillator and photo cathode of the photo-multiplier were shielded from uncollimated, low energy radiation by a housing made from lead with a hole c 0.25cm (radius)in the front face to allow the collimated beam to enter the scintillator.

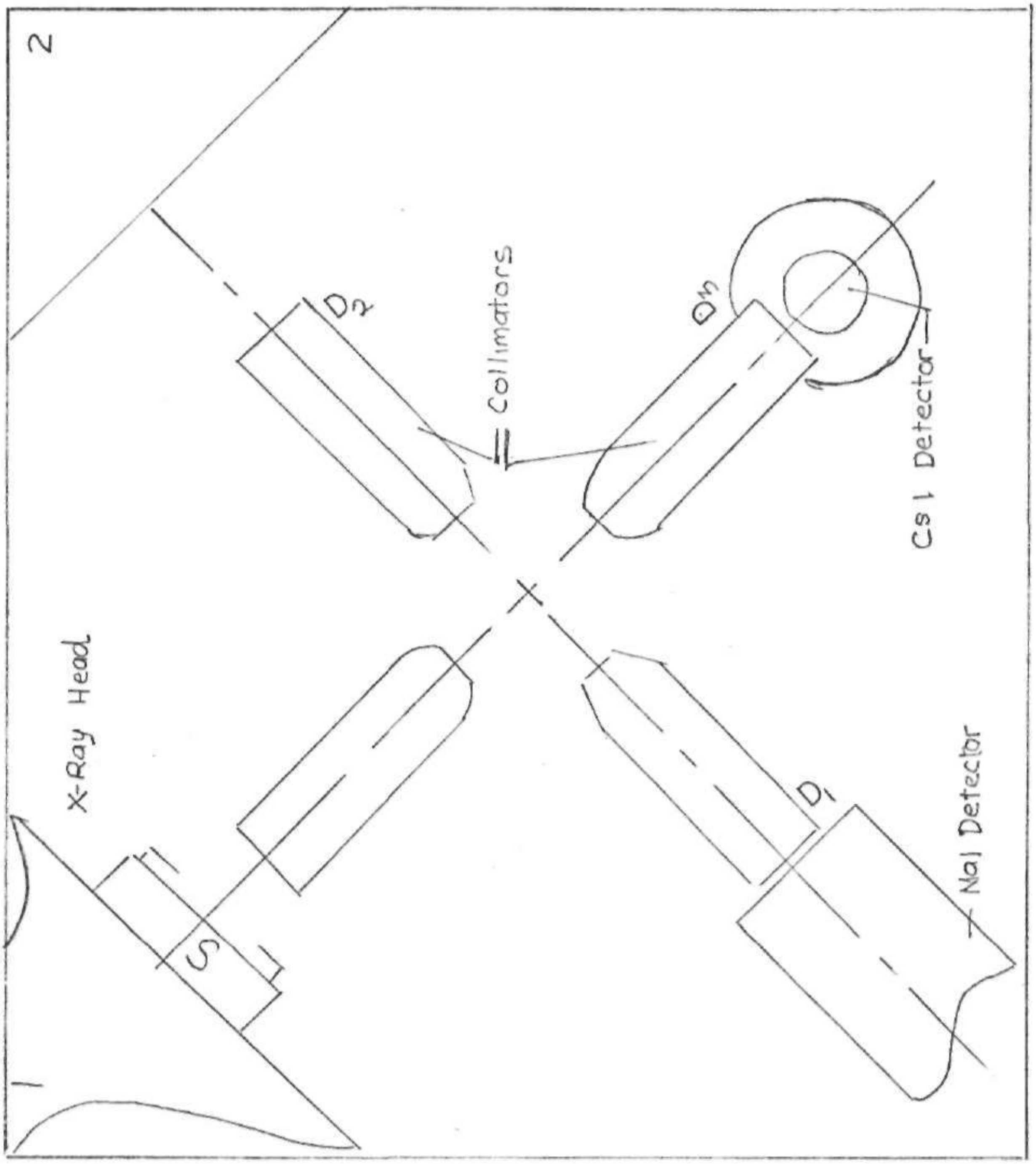

From: MORTIMER (21) ...

Fig.3-1: Front Plan of Experimental Apparatus

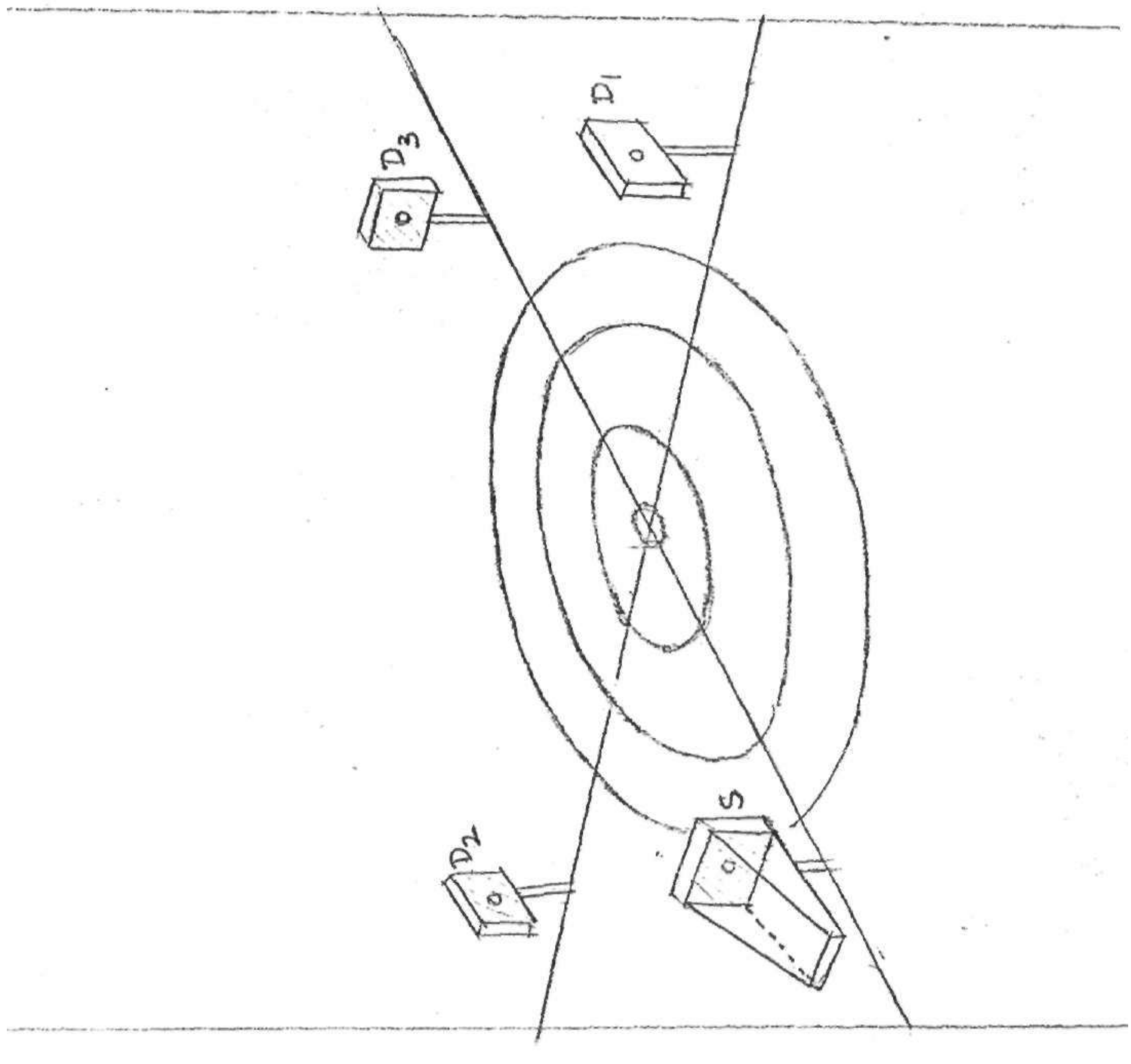

Fig.3-2: Isometric View of Experimental Apparatus

The counting electronics consisted of amplifiers, discriminators and scalers for the photomultipliers. The circuit block diagram is shown in fig.3-3. The outputs of the scattered detector photomultiplier tubes PM1 and PM2 were fed into the inputs of an Ortec 410 multimode amplifier via a switch box S. With the switch at position 1 corresponding to source position 1 in fig. 3-1, the photomultiplier tube PM1 of detector D_1 was connected to the scaler circuit; while with the switch at position 2, corresponding to source position 2, the photomultiplier tube PM2 of detector D_2 was connected to the scaler circuit. The output of the 410 multimode amplifier was connected to an Ortec 429 discrimmator scaler via single channel analyzer. The output of the unscattered detector photomultiplier tube PM3 was fed into the input of an AN 201/N Quad amplifier whose output was connected to a Nuclear Counter via a T105/N dual discriminator. The scalers were gated by gate generators. A single start push button located at a timer unit started both the electronics and the X-ray unit. The timer unit also incorporated a light device which served as an exposure indicator.

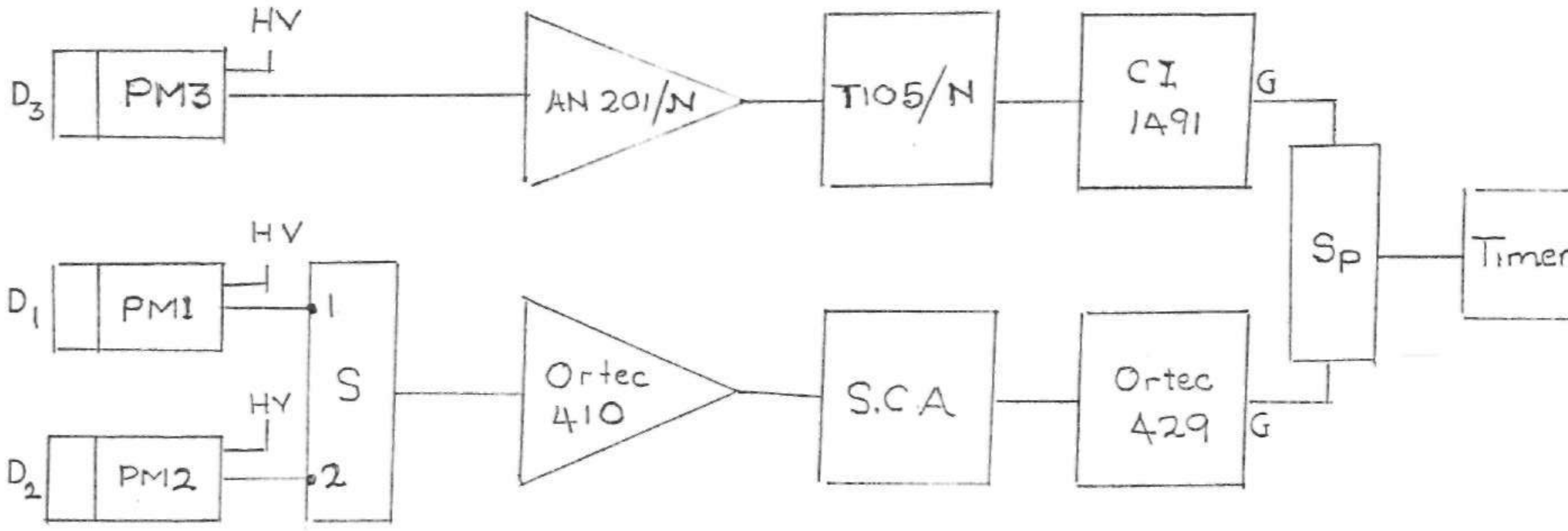

Fig.3-3: Circuit Block Diagram

PM are Phototubes
S is a Switch Box
S_p is a Splitter
S.C.A. is a Single Channel Analyser
G is a Scaler Gate

4 MULTIPLE SCATTERING

The theory of Compton scatter densitometry assumes that finite geometry, multiple and coherent scattering effects are negligible. While the contributions from these effects may fall within the precision of the measurement made for some incident photon energies (for example 412, 1173 and 1250 keV [6,17]), the validity of these assumptions become questionable for low incident photon energies ($E<150keV$) [13,18, 28].

Kennett and Webber [18] have shown that geometric and multiple scattering effects would lead to a falsely high value of density. They have also demonstrated by both calculation and experimental investigation that geometry effects are responsible for only a small fraction of the total error while multiple scattering effects are significant. Mortimer [21] has shown from experimental studies that about 1% to 19% of the scattered radiation detected is due to photons suffering more than one scattering interaction. The multiple scattered photons result in a falsely high scattered count rate. The amount of multiple scattering will depend on the dimensions and the density of the scatterer.

The need for a theoretical evaluation of multiple scattering intensity which would enable corrections to be made on any measurements taken with the Compton densitometer has thus arisen. Kennett and Webber [18] have indicated that the multi-dimensional nature of the problem in question precludes the use of the Monte Carlo simulation technique, and that a correction factor can be derived from the information collected during the density measurements. They showed that since for any object, the degree of multiple scattering and transmission of photons both depend upon the density and the dimensions of the object, the correction factor can be obtained from the transmission measurements of the lower energy photon source. In the analysis presented in this text a correction factor is derived from the scattering measurement. Since the effect of coherent scattering also becomes important for low-energy photons [9,16] the coherent scattering cross-section has also been included in the scattering analysis.

The effect of coherent scattering will be discussed in the next chapter. In this chapter we shall derive a mathematical expression for a special case of multiple scattering.

MATHEMATICAL EXPRESSION FOR DOUBLE SCATTERING

The multiple-scattered photon is one that has suffered more than one single scattering interaction within the sample in the process of transmission from source to detector. For samples with large dimensions compared to the dimensions of the collimator of the detector the physics of the system may discriminate against triple and higher order scatterings since the path length travelled by photons increases with the order of scattering and consequently attenuation takes its toll [9]. The above statement may also approximately hold for samples whose dimensions are small or comparable to that of the collimator since the probability of escape of the photon from the sensitive volume will increase with the order of scattering. We shall therefore consider only double scattering which is the simplest case of multiple scattering.

The probability of photon energy being scattered through any given angle θ is described by the Klein-Nishina differential energy scattering cross-section (per electron) per unit solid angle about θ, which is given by [9]

$$\frac{d\sigma}{d\Omega}(\text{incoh}) = \frac{1}{2} r_o^2 \, P \quad (1-P\sin^2\theta+P^2)(\text{cm}^2/\text{electron/steradian})$$

where $\sigma(\text{incoh})$ refers to the electronic Compton cross-section, $r_o = e^2/mc^2$ is the classical electron radius and P is as defined in Equation (2-1).

If we assume isotropic scattering, the Klein-Nishina cross-section per electron will be given approximately by

$$\sigma(\text{incoh}) = 4\pi \frac{d\sigma}{d\Omega}(\text{incoh})$$

For low-energy photons the total scattering cross-section is given by

$$\sigma = \sigma(\text{incoh}) + \sigma(\text{coh})$$

We wish to consider the radiation from an X-ray source at Q which is first scattered by the electrons in the infinitesimal volume dv_1 to a second volume element dv_2 and then subsequently scattered to a detector located at P as shown in fig. 4-1. The experimental set up of the system under consideration (figs. 3-1 and 3-2) has greatly simplified the formidable mathematics involved.

If we neglect the build-up factor [9] the intensity incident upon the volume element dv_1 is given by

$$I_1 = I_o \, e^{-\mu_1 (R+X_1)} \qquad \text{(for a Collimated beam)}$$

The counting rate observed at P due to the radiation scattered through angles θ_1 and θ_2 within volume elements dv_1 and dv_2 respectively will be

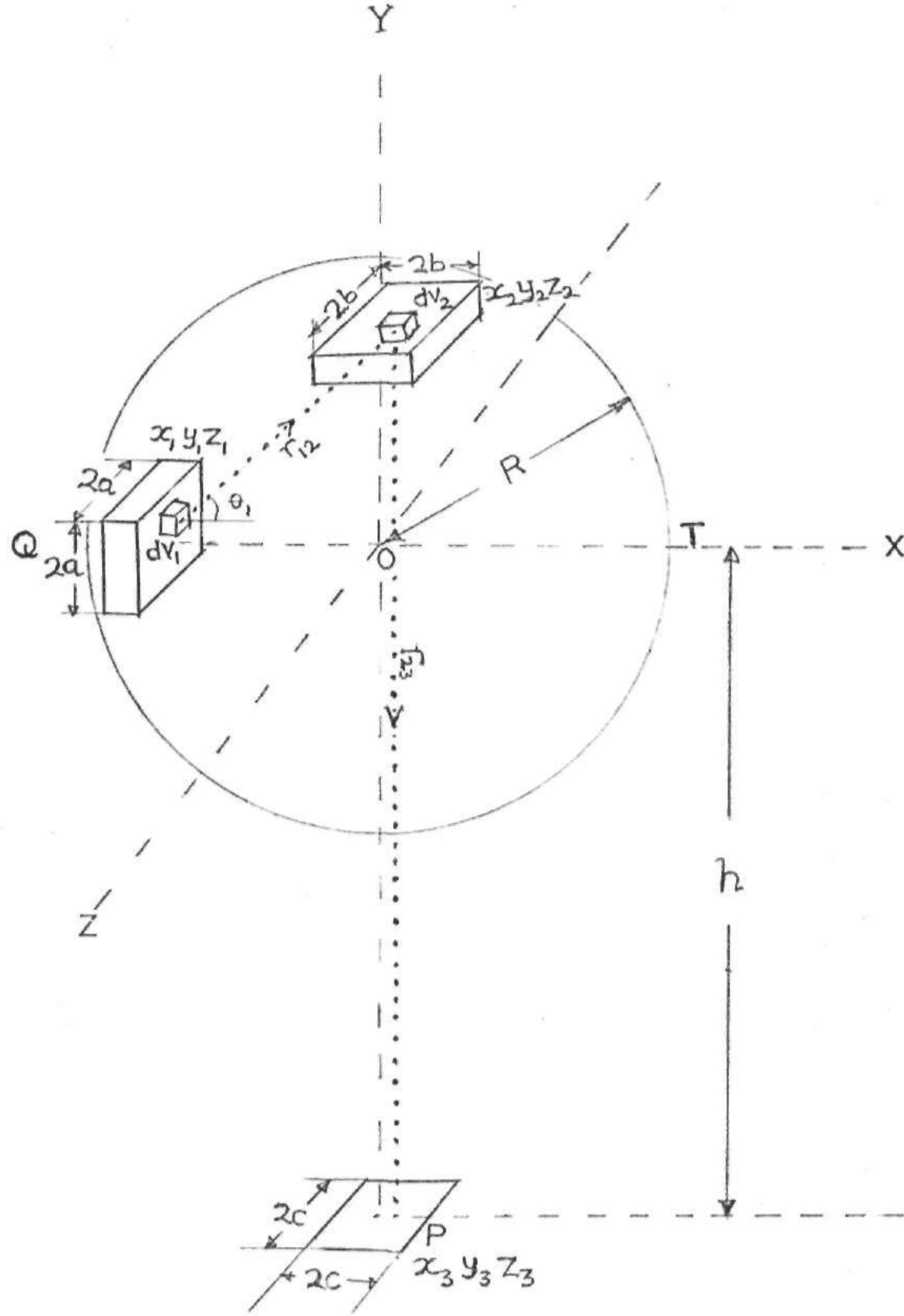

Fig.4-1: Model for the Analysis of Double Scattering

given by

$$dC_d = I_o N\sigma(\theta_1) e^{-\mu_o(R+X_1)} \frac{e^{-\mu_1(r_{12})}}{4\pi r_{12}^2} \Delta v_1 \quad X$$

$$X \; N\sigma(\theta_2) \; e^{-\mu_2(R+Y_2)} \Delta v_2 \frac{\Delta A}{4\pi r_{23}^2} \qquad (4\text{-}1)$$

Where I_o is the intensity of the incident beam (photons - sec^{-1}- Cm^{-2})

N is the electron density of the sample.

$$N = Z \frac{(\text{electrons})}{(\text{atom})} N_a \frac{(\text{atoms})}{(\text{mole})} \rho \frac{(\text{gm})}{(\text{cm}^3)} \frac{1}{A} \frac{(\text{mole})}{(\text{gm})}$$

where Z is the atomic number, N_a is Avagadro's number, ρ is the density and A is the atomic mass of the sample.

$\Delta v_1 = dx_1 \; dy_1 \; dz_1$

$\Delta v_2 = dx_2 \; dy_2 \; dz_2$

$\Delta A = dx_3 \; dz_3$

$r_{12}^2 = (x_1-x_2)^2 + (y_1-y_2)^2 + (z_1-z_2)^2$

$r_{23}^2 = (x_2-x_3)^2 + (y_2+h)^2 + (z_2-z_3)^2$

μ_1 and μ_2 are the total linear attenuation coefficients for the incident and scattered beam [8,9]

<u>SIMPLIFYING ASSUMPTIONS</u>: To reduce the mathematical complexity of the analysis we make the following assumptions.

(i) For the energies of interest (30-90 kev) in the present consideration we can assume at 45^0

$$\sigma(\theta_1) = \sigma(\theta_2) \approx \frac{\sigma}{4\pi}$$

where σ is the total scattering cross-section.

(ii) Also $h > R$; $R >> a,b,c$

$$|x_2 - x_3| \leq |b+c| << h$$

$$|z_2 - z_3| \leq |b+c| << h$$

so that $r_{23}^2 = (h + y_2)^2$

Over the region of interest $b^2 \alpha \ (h+y_2)^2$ and since $h > R$, we can substitute h^2 for $(h + y_2)^2$. The error introduced will to a first order cancel out.

(iii) For simplicity assume $\mu_1 = \mu_2$ and that the absorption of the gamma radiation in air is negligible.

The total counting rate at the detector as a result of double scattering is obtained by integration over all Δv_1's and Δv_2's from which double scattering can occur. With the inclusion of the above assumptions the total counting rate is given by

$$C_d = \frac{I_o N^2 \sigma^2 A}{16\pi^2 h^2} \int_{x_1=-R}^{+R} \int_{y_1=-a}^{+a} \int_{z_1=-a}^{+a} \int_{x_2=-b}^{+b} \int_{y_2=-R}^{+R} \int_{z_2=-b}^{+b} (\text{Integrand}$$

where

$$\text{Integrand} = \frac{\exp(-\mu[\sqrt{(x_1-x_2)^2+(y_1-y_2)^2+(z_1-z_2)^2}+(R+x_1)+(R+y_2)])}{\left[(x_1-x_2)^2 + (y_1-y_2)^2 + (z_1-z_2)^2\right]}$$

$$X \quad dx_1 \; dy_1 \; dz_1 \; dx_2 \; dy_2 \; dz_2$$

and $\quad A = \iint dx_3 \; dz_3$

To simplify the above expression consider the change of variable [26] defined by

$$\begin{bmatrix} x \\ u \end{bmatrix} = g^{-1} (x_1, x_2) = \frac{1}{\sqrt{2}} \begin{bmatrix} x_1 - x_2 \\ x_1 + x_2 \end{bmatrix}$$

$$\iint dx_1 \; dx_2 = \iint \left| \frac{\partial(x_1, x_2)}{\partial(x, u)} \right| dx \; du$$

but

$$\frac{\partial(x_1, x_2)}{\partial(x, u)} = \left(\frac{\partial(x, u)}{\partial(x_1, x_2)}\right)^{-1} = \begin{vmatrix} \frac{\partial x}{\partial x_1} & \frac{\partial x}{\partial x_2} \\ \frac{\partial u}{\partial x_1} & \frac{\partial u}{\partial x_2} \end{vmatrix}^{-1} = 1$$

Similarly

Let $\begin{bmatrix} y \\ v \end{bmatrix} = g^{-1}(y_1, y_2) = \frac{1}{\sqrt{2}} \begin{bmatrix} y_1 - y_2 \\ y_1 + y_2 \end{bmatrix}$

$$\begin{bmatrix} z \\ w \end{bmatrix} = g^{-1}(z_1, z_2) = \frac{1}{\sqrt{2}} \begin{bmatrix} z_1 - z_2 \\ z_1 + z_2 \end{bmatrix}$$

then $\dfrac{\partial(y_1, y_2)}{\partial(y, v)} = 1$ and $\dfrac{\partial(z_1, z_2)}{\partial(z, w)} = 1$

so that

$$\int_{x_1}\int_{y_1}\int_{z_1}\int_{x_2}\int_{y_2}\int_{z_2} dx_1 dy_1 dz_1 dx_2 dy_2 dz_2 = \int_x\int_y\int_z\int_u\int_v\int_w dx\,dy\,dz\,du\,dv\,dw$$

The expression for the total counting rate then reduces to

$$C_d = \frac{I_o N^2 \sigma^2 A e^{-2\mu R}}{16\pi^2 h^2} \int_x\int_y\int_z\int_u\int_v\int_w \frac{\exp(-\mu[\sqrt{2(x^2+y^2+z^2)} + x_1 + x_2])\,dx\,dy\,dz\,du\,dv\,d}{2(x^2 + y^2 + z^2)}$$

(4-2)

To make the mathematical problem tractable the following assumptions are made.

First, we assume that far away from the origin ($|b/\sqrt{2}| < |x| < |R/\sqrt{2}|$ and $|a/\sqrt{2}| < |y| < |R/\sqrt{2}|$),

$X = \frac{1}{\sqrt{2}}(x_1 - x_2) \approx \frac{1}{\sqrt{2}} x_1$; and $y \approx \frac{1}{\sqrt{2}} y_2$.

Second, we assume that near the origin ($0 < |x| < |b|\sqrt{2}|$ and $0 < |y| < |a/\sqrt{2}|$, the range of values of both x_1 and y_2 is very small so that

$x_1 \approx x_2 \approx x \approx 0$ and $y_1 \approx y_2 \approx y \approx 0$ and thus we can neglect these terms in the exponent. This latter approximation permits the use of spherical co-ordinates to remove the singularity at the origin. The approximate exponential term in equation (4-2) becomes $\exp(-\sqrt{2}\mu(\sqrt{x^2+y^2+z^2}+x+y)$ far away from the origin and $\exp(-\sqrt{2}\mu(\sqrt{x^2+y^2+z^2})$ near the origin.

Limits:

The original limits were specified as

$-R<x_1<R \qquad -a<y_1<a \qquad -a<z_1<a$

$-b<x_2<b \qquad -R<y_2<R \qquad -b<z_2<b$

The limits of the new variables x,y,z,u,v and w were determined as shown in fig. 4-2(i). To simplify the mathematical analysis the integration was over a parallelogram (shaded region in fig. 4-2(i)) which has the same area as the rectangular region of interest.

The approximate expression for C_d was obtained as

$$C_d = \frac{I_o N^2 \sigma^2 A e^{-2\mu R}}{32\pi^2 h^2} \left[IxuIyvIzw \frac{\exp(-\sqrt{2}\mu(\sqrt{x^2+y^2+z^2}+x+y)}{x^2+y^2+z^2} \right]$$

where $$Ixu = \int_{-R/\sqrt{2}}^{R/\sqrt{2}} dx \int_{u=x-b/\sqrt{2}}^{u=x+b/\sqrt{2}} du$$

$$Iyv = \int_{-R/\sqrt{2}}^{R/\sqrt{2}} dy \int_{v=y+a/\sqrt{2}}^{v=y-a/\sqrt{2}} dv$$

$$Izw = \int_{-b/\sqrt{2}}^{b/\sqrt{2}} dz \int_{w=z+a/\sqrt{2}}^{w=z-a/\sqrt{2}} dw$$

thus

$$Cd = \frac{\sqrt{2} I_o N^2 \sigma^2 A e^{-2\mu R} a^2 b}{2\pi^2 h^2} \int_{-R/\sqrt{2}}^{R/\sqrt{2}} \int_{-R/\sqrt{2}}^{R/\sqrt{2}} \int_{-b/\sqrt{2}}^{b/\sqrt{2}} \frac{\exp(-\sqrt{2}\mu(\sqrt{x^2+y^2+z^2}+x+y)\,dx\,dy\,dz}{x^2+y^2+z^2}$$

Let $k = \sqrt{2} I_o N^2 \sigma^2 A a^2 / 2\pi^2 h^2$ (Photons sec^{-1} cm^{-2})

In terms of the assumptions discussed above C_d can be expressed as

$$C_d = \begin{cases} C_d' = kbe^{-2\mu R} \int_x \int_y \int_z \dfrac{\exp(-\sqrt{2}\mu(\sqrt{x^2+y^2+z^2}+x+y)\,dx\,dy\,dz}{x^2+y^2+z^2} & \text{away from the origin} \\ C_d'' = kbe^{-2\mu R} \int_x \int_y \int_z \dfrac{\exp(-\sqrt{2}\mu(\sqrt{x^2+y^2+z^2})\,dx\,dy\,dz}{x^2+y^2+z^2} & \text{near the origin} \end{cases}$$

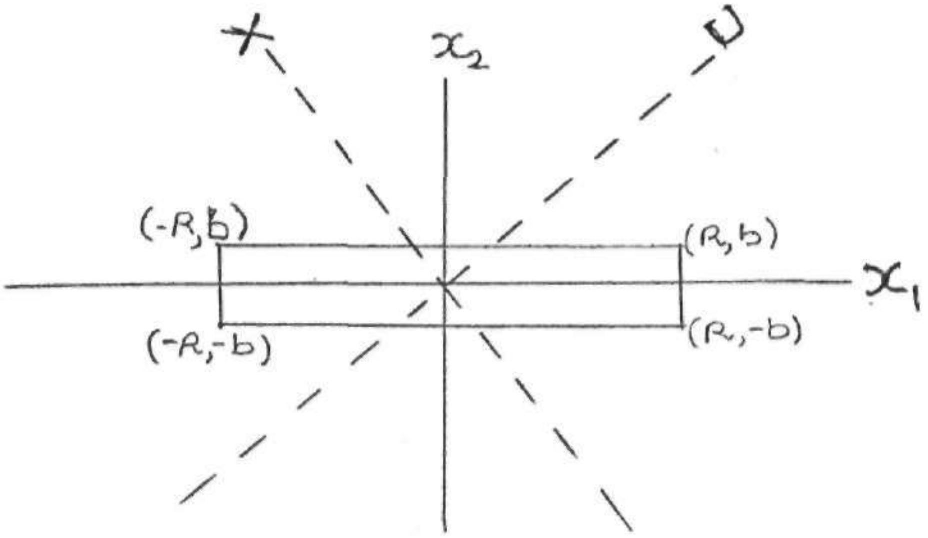

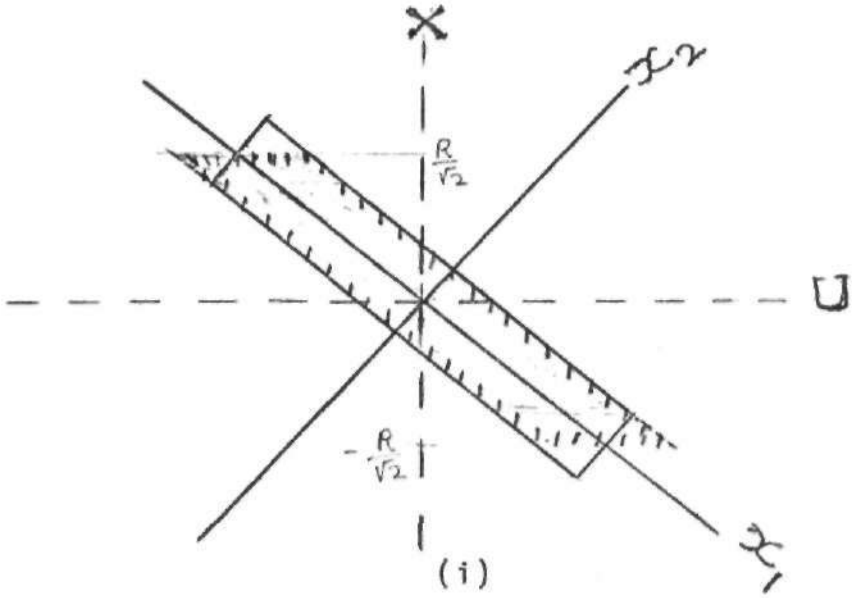

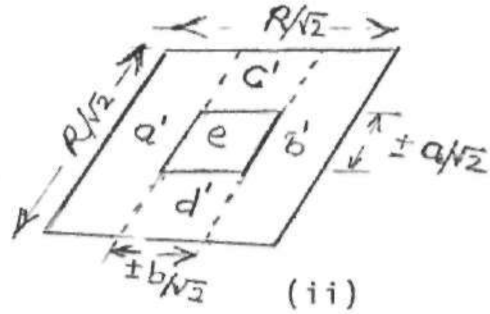

Fig. 4-2: Model for Mathematical Analysis
(i) Evaluation of Limits of Integration
(ii) Subdivision of Region of Integration (Not Drawn to Scale)

We shall now consider the analysis of the above expressions

(i) For the region far from the origin:

$$C_d' = kbe^{-2\mu R}\int_x\int_y\int_z \frac{\exp(-\sqrt{2}\mu(\sqrt{x^2+y^2+z^2}+x+y)dxdydz}{x^2+y^2+z^2} \tag{4-3}$$

To evaluate this expression the integral region was subdivided into four parts as shown in fig. 4-2 (ii) as follows

$$C_d'[a'] = k'\int_{-R/\sqrt{2}}^{-b/\sqrt{2}}\int_{-R/\sqrt{2}}^{R/\sqrt{2}}\int_{-b/\sqrt{2}}^{b/\sqrt{2}}(\text{Integrand})$$

$$C_d'[b'] = k'\int_{b/\sqrt{2}}^{R/\sqrt{2}}\int_{-R/\sqrt{2}}^{R/\sqrt{2}}\int_{-b/\sqrt{2}}^{b/\sqrt{2}}(\text{Integrand})$$

$$C_d'[c'] = k'\int_{-b/\sqrt{2}}^{b/\sqrt{2}}\int_{a/\sqrt{2}}^{R/\sqrt{2}}\int_{-b/\sqrt{2}}^{b/\sqrt{2}}(\text{Integrand})$$

$$C_d'[d'] = k'\int_{-b/\sqrt{2}}^{b/\sqrt{2}}\int_{-R/\sqrt{2}}^{-a/\sqrt{2}}\int_{-b/\sqrt{2}}^{b/\sqrt{2}}(\text{Integrand})$$

where $k' = kbe^{-2\mu R}$,

and

$$\text{integrand} = \frac{\exp(-\sqrt{2}\mu(\sqrt{x^2+y^2+z^2}+x+y)dxdydz}{x^2+y^2+z^2}$$

The above integrals were evaluated by numerical integration. The Gaussian quadrature formula [19,25] was used because it provides accurate results when finding the value of the definite integral

$$I = \int_A^B f(x)\, dy$$

where f(x) is a known function but whose integral is either not easily evaluated or cannot be conveniently expressed in closed form. The first step in this method is to transform the interval (A,B) to the interval (-1,1) which is easily accomplished by the change of variable

$$X = \frac{(B-A)t + (B+A)}{2}; \quad dx = \frac{(B-A)}{2}\, dt$$

The new form of f(x) is thus

$$f(x) = f\left[\frac{(B-A)t + (B+A)}{2}\right]$$

The N-point Gaussian integration formula is given by

$$\int_A^B f(x)\, dx = \frac{B-A}{2} \sum_{i=1}^{N} w_i f\left(\frac{(B-A)t_i + (B+A)}{2}\right)$$

where $w_1, w_2 + \ldots\ w_n$ are weighing coefficients and $t_1, t_2, \ldots t_n$ are the roots of the legendre polynomials. In terms of the Gaussian quadrature formula the integral of region a', as shown in fig. 4-2(ii), can be expressed as

$$C_d'[a'] = \beta \sum_{i=1}^{N} \sum_{j=1}^{N} \sum_{k=1}^{N} w_i w_j w_k f\left[\frac{((R-b)t_i - (R+b)}{2\sqrt{2}}, \frac{Rt_j}{\sqrt{2}}, \frac{(b)t_k}{\sqrt{2}}\right]$$

where $\beta = k' \frac{(R-b)}{2\sqrt{2}} \frac{(R)}{\sqrt{2}} \frac{(b)}{\sqrt{2}}$

The integrals were all evaluated using N=32. As expected the computer analysis showed a variation in the magnitude of the contributions from the various regions.

(ii) For the region close to the origin

$$C_d'' = kbe^{-2\mu R} \int_{-b/\sqrt{2}}^{b/\sqrt{2}} \int_{-a/\sqrt{2}}^{a/\sqrt{2}} \int_{-b/\sqrt{2}}^{b/\sqrt{2}} \frac{\exp(-\sqrt{2}\mu\sqrt{x^2+y^2+z^2})dxdydz}{x^2+y^2+z^2} \quad \ldots (4\text{-}4)$$

The integrand (4-4) is singular at the origin. To remove the singularity, we make the co-ordinate transformation:

$X = r\sin\phi\cos\theta$, $y = r\sin\phi\sin\theta$ $\quad z = r\cos\phi$

$dxdydz = r^2 \sin\phi \, drd\phi d\theta$

so that

$$C_d'' = 2\pi kbe^{-2\mu R}\left[\int_{\phi_o}^{\pi-\phi_o} \int_0^{P(\phi)} e^{-\sqrt{2}\mu r}\sin\phi drd\phi + 2\int_0^{\phi_o}\int_0^{Q(\phi)} e^{-\sqrt{2}\mu r}\sin\phi drd\phi\right]$$

where $P(\phi) = D\,\mathrm{cosec}\phi$; $\phi_o = \tan^{-1}D/(b/\sqrt{2})$; $Q(\phi) = b(\mathrm{Sec}\phi)/\sqrt{2}$

$D = (2b^2/\pi)^{1/2}$ is the radius of a circular disc which will give the same volume as a cuboid of side $2b/\sqrt{2}$ ($a \approx b$ for the configuration in question).

$$\text{or } C_d'' = \frac{2\pi k'}{\mu}\int_{\phi_o}^{\pi-\phi_o}(1-e^{-\sqrt{2}\mu D/\sin\phi})\sin\phi d\phi \quad + C_d''' \quad \ldots\ldots \quad (4\text{-}5)$$

where $k' = kbe^{-2\mu R}$ and $C_d''' = 4\pi kbe^{-2\mu R}\int_0^{\phi_o}\int_0^{\phi(\phi)} e^{-\sqrt{2}\mu r}\sin\phi dr d\phi$

Integral 4-5 was also evaluated by a 32-point Gaussian quadrature formula. The integral corresponds to the portion marked "e" in fig. 4-2 (ii).

The total contribution due to double scattering at P is thus

$$C_d = C_d' + C_d''$$

$$= C_d'[a'] + C_d'[b'] + C_d'[c'] + C_d'[d'] + C_d''$$

In order to compare the contribution due to double scattering to the contributions due to single scattering and unscattered events respectively, it is necessary to derive similar expressions for the latter cases. The amount of correction to be applied to the observed data will be extracted from the observed scattered counts and this will come from a knowledge of the ratio of the double to single scattered photons.

SINGLE SCATTERING:

The single scattering events take place within the sensitive volume which is defined by the Collimator geometry.

The incident intensity upon the volume element dv_1 at O is given by

$$I_s = I_o e^{-\mu R}$$

The counting rate observed at the counter at P due to the radiation scattered within the volume element dv_1 at O is

$$dC_s = I_o e^{-\mu R} N\sigma \frac{e^{-\mu R}}{4\pi h^2} \Delta v_1 \Delta A$$

where $\Delta v_1 = dx_1 dy_1 dz_1$

$$\Delta A = dx_3 dz_3$$

The total counting rate observed at P is obtained by integration over all volume elements from which single scattering can occur

$$C_s = \frac{I_o N\sigma e^{-2\mu R} A}{4\pi h^2} \int_{-b}^{b} \int_{-a}^{a} \int_{-a}^{a} dx_1 dy_1 dz_1$$

$$C_s = I_o N\sigma A 8a^2 b e^{-2\mu R} / 4\pi h^2$$

As in the case of double scattering if we let

$k = \sqrt{2}\ I_o N^2\sigma^2 A a^2/2\pi^2 h^2$, then

$C_s = 2\sqrt{2\pi} k b e^{-2\mu R}/N\sigma$

$$C_s = 2\sqrt{2\pi} k'/N\sigma \qquad (4\text{-}6)$$

UNSCATTERED OR TRANSMITTED PHOTONS

The scattered and transmitted detectors are equidistant from the sensitive volume so that the transmitted intensity at a position T in Fig.4-1, will be given by

$C_T = A''\ I_o e^{-2\mu R}$

where A" is the cross-sectional area of the incident beam at the transmitted detector.

thus

$$C_T = \frac{A''\sqrt{2}\pi^2 k}{N^2\sigma^2 a^2} e^{-2\mu R}\ \frac{h^2}{A}$$

$$C_T = \frac{A''\sqrt{2}\pi^2 k'}{N^2\sigma^2 a^2 b}\ \frac{h^2}{A} \qquad (4\text{-}7)$$

SUMMARY OF CALCULATION:

From the foregoing analysis, the ratios of the double scattered to the single scattered and the transmitted photon beam are respectively given by

$$\frac{C_d}{C_s} = \frac{\sqrt{2}N\sigma}{4\pi} \int_{-R/\sqrt{2}}^{R/\sqrt{2}} \int_{-R/\sqrt{2}}^{R/\sqrt{2}} \int_{-b/\sqrt{2}}^{b/\sqrt{2}} \frac{\exp(-\sqrt{2}\mu(\sqrt{x^2+y^2+z^2}+x+y)\,dx\,dy\,dz}{x^2+y^2+z^2}$$

(4-8)

$$\frac{C_d}{C_T} = \frac{\sqrt{2}b(N\sigma)^2 a^2 \gamma}{2\pi^2 A''} \int_{-R/\sqrt{2}}^{R/\sqrt{2}} \int_{-R/\sqrt{2}}^{R/\sqrt{2}} \int_{-b/\sqrt{2}}^{b/\sqrt{2}} \frac{\exp(-\sqrt{2}\mu(\sqrt{x^2+y^2+z^2}+x+y)\,dx\,dy\,dz}{x^2+y^2+z^2}$$

(4-9)

where $\gamma = \frac{A}{h^2}$

For the present system $A = 0.25\text{cm}^2$ and $h = 17.0\text{cm}$ so that the quantity γ is approximately 10^{-3}.

5 COHERENT SCATTERING

Also important at low energies is coherent (Rayleigh) scattering, a process in which the photon is deflected by the atomic electron with no loss in energy[16]. In Compton scattering the interaction takes place with a loosely bound electron, resulting in an energy loss in the scattered photon governed by the well-known Compton equation of atomic physics. In Rayleigh scattering an incident photon interacts with a tightly bound atomic electron and thereby is elastically scattered with no loss of energy. The photon scattered by either of these processes can reach the detector and contribute to the counts recorded in the counter [30]. The magnitude of the contributions will be dependent on the photon energy and the atomic number Z of the substance being examined. The coherent cross-section is proportional to $Z^{\sim 2-3}$ [28].

The existing Compton scattering densitometry equation only utilizes the Compton or incoherent scattering cross-section and assumes that the coherent scattering cross-section is negligible. While this assumption may be valid for the low Z elements, for high Z elements the contribution from coherent scattering becomes very significant to be neglected. For example, the chemical composition of bone known as hydroxyapatite has a chemical formula $Ca_{10}(PO_4)_6(OH)_2$ [21]. While the ratio of the coherent to the incoherent cross-section for hydrogen and oxygen may be negligible in the energy range of interest this ratio is about 60% for Calcium (Z=20) and about 39% for phosphorus (Z=15)[16] and may thus introduce considerable error if completely neglected.

If σ_e is the cross-section per electron, then the relativ electron density D_e for the case where σ_e is not a a function of Z, is given by

$$D_e = \frac{(\rho_e \sigma_e)_x}{(\rho_e \sigma_e)_s} = \frac{(\rho_e \sigma_e^{incoh})_x}{(\rho_e \sigma_e^{incoh})_s} = \left[\frac{(S_1 S_2/T_1 T_2)_x}{(S_1 S_2/T_1 T_2)_s}\right]^{1/2} \qquad (5\text{-}1)$$

Equation (5-1) is the basis of the original densitometry theory [6].

If, however, σ_e is a function of Z the scattering cross-section per electron becomes

$\sigma_e = \sigma_e^{incoh} + \sigma_e^{coh}$ and

$$D_e = \frac{\left(\rho_e\left(\sigma_e^{incoh} + \sigma_e^{coh}\right)\right)_x}{\left(\rho_e\left(\sigma_e^{incoh} + \sigma_e^{coh}\right)\right)_s}$$

$$D_e = \underbrace{\underbrace{\frac{\left(\rho_e \sigma_e^{incoh}\right)_x}{\left(\rho_e \sigma_e^{incoh}\right)_s}}_{\text{original}} \left[\frac{1 + \left(\dfrac{\sigma_e^{coh}}{\sigma_e^{incoh}}\right)_x}{1 + \left(\dfrac{\sigma_e^{coh}}{\sigma_e^{incoh}}\right)_s}\right]}_{\text{Proposed}} \qquad (5\text{-}2)$$

$$D_e = \frac{(Z/A)_x \, (\rho_x)}{(Z/A)_s \, (\rho_s)_A} \left[\frac{1 + \alpha_x}{1 + \alpha_s}\right]$$

$$\rho_x = D_e (A/Z)_x (Z/A)_s \left[\frac{1 + \alpha_s}{1 + \alpha_x}\right] (\rho_s)_A \qquad (5\text{-}3)$$

where

$$D_e = \left[\frac{(S_1 S_2 / T_1 T_2)_x}{(S_1 S_2 / T_1 T_2)_s}\right]^{1/2}$$

and

$$\alpha_x = \left[\sigma_\varepsilon^{coh} / \sigma_e^{incoh}\right]_x \qquad \alpha_s = \left[\sigma_e^{coh} / \sigma_e^{incoh}\right]_s$$

Fitzgerald et al [9] has indicated that in the energy range [20 KeV to 10 MeV],coherent scattering is confined primarily to small angles in practice. Since the present Compton scatter densitometer utilizes a single scattering angle of 90°, the proposed equation 5-2 reduces to the original formulation. However, for other configurations which utilize scattering angles much less than 90°, Equation 5-2 may become useful.

6 MEASUREMENT PROCEDURE

A number of experiments were performed to compare

(1) the calculations on double scattering with experiment

(2) the results of the corrected densities obtained with the Compton densitometer with the actual densities found by gravimetric methods.

The measurement procedure was relatively simple. To measure the electron density of an object, the object was placed centrally at the sensitive region. The collimated photon beam from the x-ray unit at the first source location (fig.3-1) was directed at the object in question and with the switch S in position 1 (fig.3-3) the Compton scattered beam was measured for an exposure time of five seconds by detector D_1 (S_1 counts) and the transmitted beam was measured by detector D_3(T_1 counts). Similar measurements were repeated after the x-ray unit had been rotated through an angle of 90^o to source location 2 and the switch S, switched to position 2. The scattered beam was then measured by detector D_2 (S_2 counts) and the transmitted beam by detector D_3. (T_2 counts). The electron density of the object within the scattering volume, after the appropriate corrections for background was then calculated from the relation

$$\rho_x = k\left[S_1 S_2/T_1 T_2\right]^{1/2}$$

The constant k was evaluated by doing the same measurement with acrylic plastic (ρ = 1.185 gm/cm^3). The computed densities were then corrected for multiple scattering using the curves derived from equation (4-8). Two to four measurements were taken at each source position.

A concise account of the experimental measurements made will be given below and this will be followed by a discussion of the experimental results in the next chapter.

(1) COMPARISON BETWEEN THEORY AND EXPERIMENT

In order to compare the results of the calculations on double scattering with experiment, scattered and transmitted photon measurements were made for a series of solid lucite $(C_5H_8O_2)_x$ cylinders of varying diameters all with a 2cm hole drilled at their centres and each cylinder was about 10cm long. The maximum dimension of the sensitive volume of the system under consideration was 1.0cm; thus the removal of a 2cm (diameter) by 9cm (height) piece of lucite rod from the centres of the lucite samples implied that the sensitive region has been detached from each of the samples examined. Under such a situation no single scattering events can occur, hence the observed counts in the scattered detector must be due to photons which have suffered more than one collision. In order to allow proper comparison to be made between the calculated and observed, lucite models similar to the ones used in the experimental measurements were used in calculating the ratio of the scattered to transmitted photons.

(2) DENSITY MEASUREMENTS:

The density measurements of aluminum (Aℓ), teflon $(C_2F_4)_x$, graphite, C, and water H_2O were made with the Compton scatter densitometer. The diameters of these samples (except water) ranged from 1.0cm to 5cm and they were all in the form of cylinders of height 10cm. Attempts to make use of a real bone model in the measurements were unsuccessful. Throughout this study lucite $(C_5H_8O_2)_x$ was used as the standard. Both the samples and the standard were given nearly equal attention since the theoretical assumptions affect both equally. The fairly wide selection of samples of different densities enabled the study of multiple scattering as a function of density to be made while the wide range of diameters considered in the measurements enabled the study of multiple scattering as a function of the dimensions of the object to be made.

Two basic methods of sample arrangement were employed in the density measurements. These methods are described below.

Method 1: Bare sample arrangement:

Two sets of density measurements were made under this method.

SET A:

In this set of density measurements the diameter of the bare samples were varied, while the diameter of the standard was fixed at some chosen value. A standard diameter of 3.0cm was chosen.

SET B:

In this set of density measurements both the diameters of the samples and the standard were varied in corresponding order so that an aluminum sample of 2.0cm diameter was standardized by a lucite standard of 2.0cm diameter.

Method 2: Simulation sample arrangement:

To simulate surrounding tissue the samples (all with a fixed diameter of 2cm) were placed in a 2cm hole drilled at the centres of solid lucite cylinders of varying diameters. Two sets of density measurements were made:

SET A':

In this set of density measurements, the outer diameters of lucite specimen surrounding the sample were varied while the diameter of the lucite standard was fixed at 4-5cm.

SET B$'$:

In this set of density measurements both the outer diameter of the surrounding lucite specimen and the standard were varied correspondingly as discussed in Set B above.

7 Results and Conclusion:

In the previous chapter a number of experiments were described. Following are the results of the various experiments.

1. RESULTS OF COMPARISON BETWEEN CALCULATION AND EXPERIMENT

The result of this experiment is presented in fig.7-1. Both the predicted curve and the experimental curve show gradual increase in the ratio of multiple scattered to transmitted photons, with increasing object diameter. However, the observed magnitude of the ratio of the multiple scattered to transmitted photons is much higher than the predicted values. The predicted curve was obtained from equation (4-9) on page 36. The discrepancy between the predicted and the observed values may be attributed to two major factors. First, we realize that the predicted curve is a measure of the ratio of double scattered to the transmitted photons while the observed curve is a measure of the ratio of the sum of the double and higher order scattered photons to the transmitted photons. Second, the air column within the 2cm hole might have some measureable affect, since air has a finite scattering cross-section [8,9]. The effect of air scattering was examined by determining the scattered and transmitted count rate with no sample present except air. The ratio of the scattered to transmitted

Table 7-1: Nuclear data [6] in the energy range of interest (30 KeV - 90 KeV)

SUBSTANCE	CHEMICAL COMPOSITION	DENSITY gm/cm3	$\frac{Z}{A}$	$\frac{A}{Z}$	$\frac{\mu}{cm}^{-1}$	INCOHERENT CROSS-SECTION BARN/ELECTRON	COHERENT CROSS-SECTION BARN/ELECTRON
Aluminum	AL	2.70	.482	2.077	.944	.49987	.12842
Lucite	$C_5H_8O_2$	1.185	.54	1.987	.234	.517025	.04490
Teflon	C_2F_4	2.138	.478	2.092	.433	.51221	.06510
Water	H_2O		.55	1.985	.216	.51396	.05698
Bone Composition (hydroxy apatite)	$Ca_{10}(PO_4)_6(OH)_2$	1.90	.4968	2.013	1.739	.49394	.18028
Graphite	C	1.66	.50	2.0	.285	.531538	.0367783

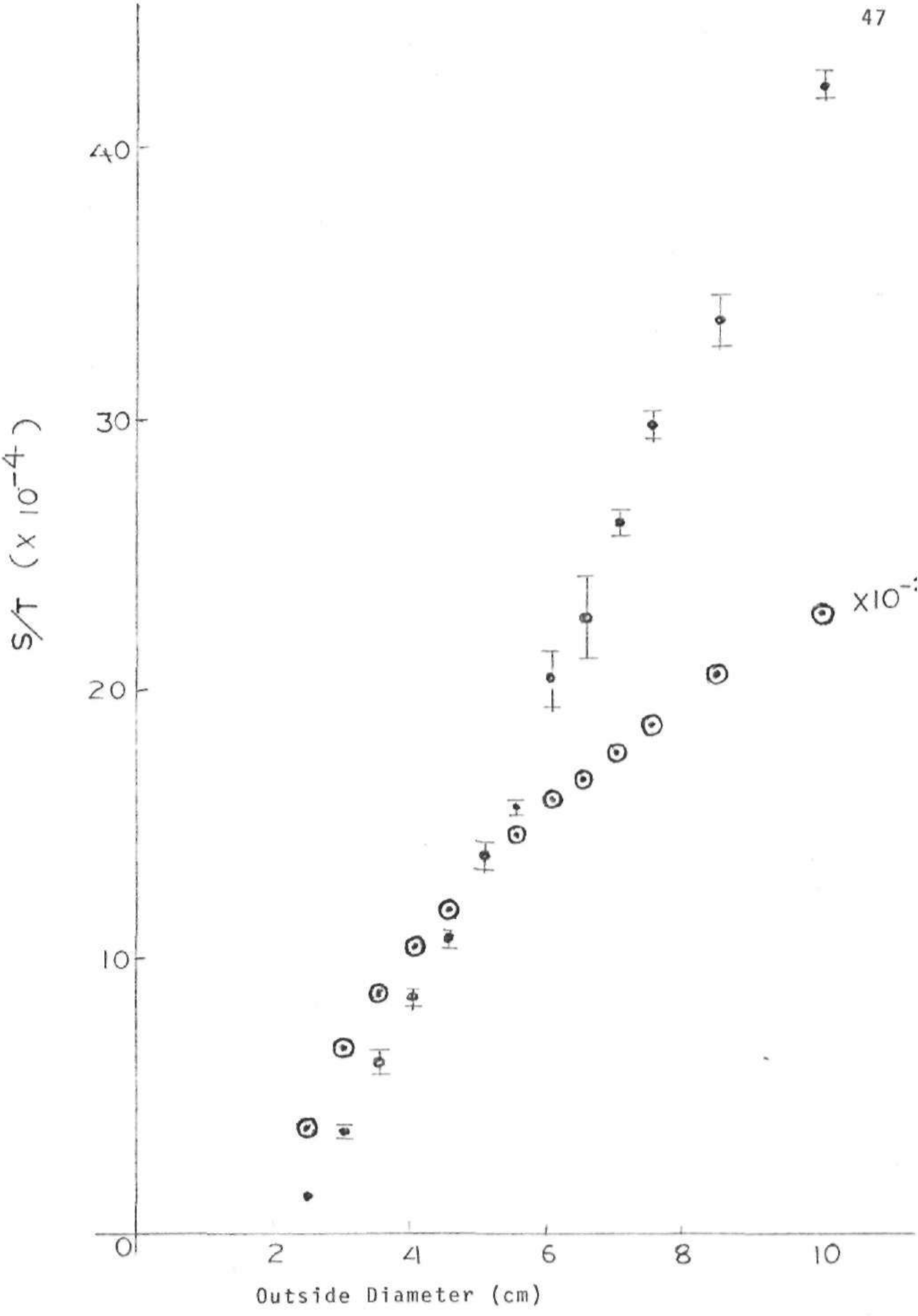

Fig.7-1: The observed (.) and predicted (⊙). Double Scattered/Transmitted intensity ratios as a function of the outside diameters of Lucite rod with a 2cm central hole.

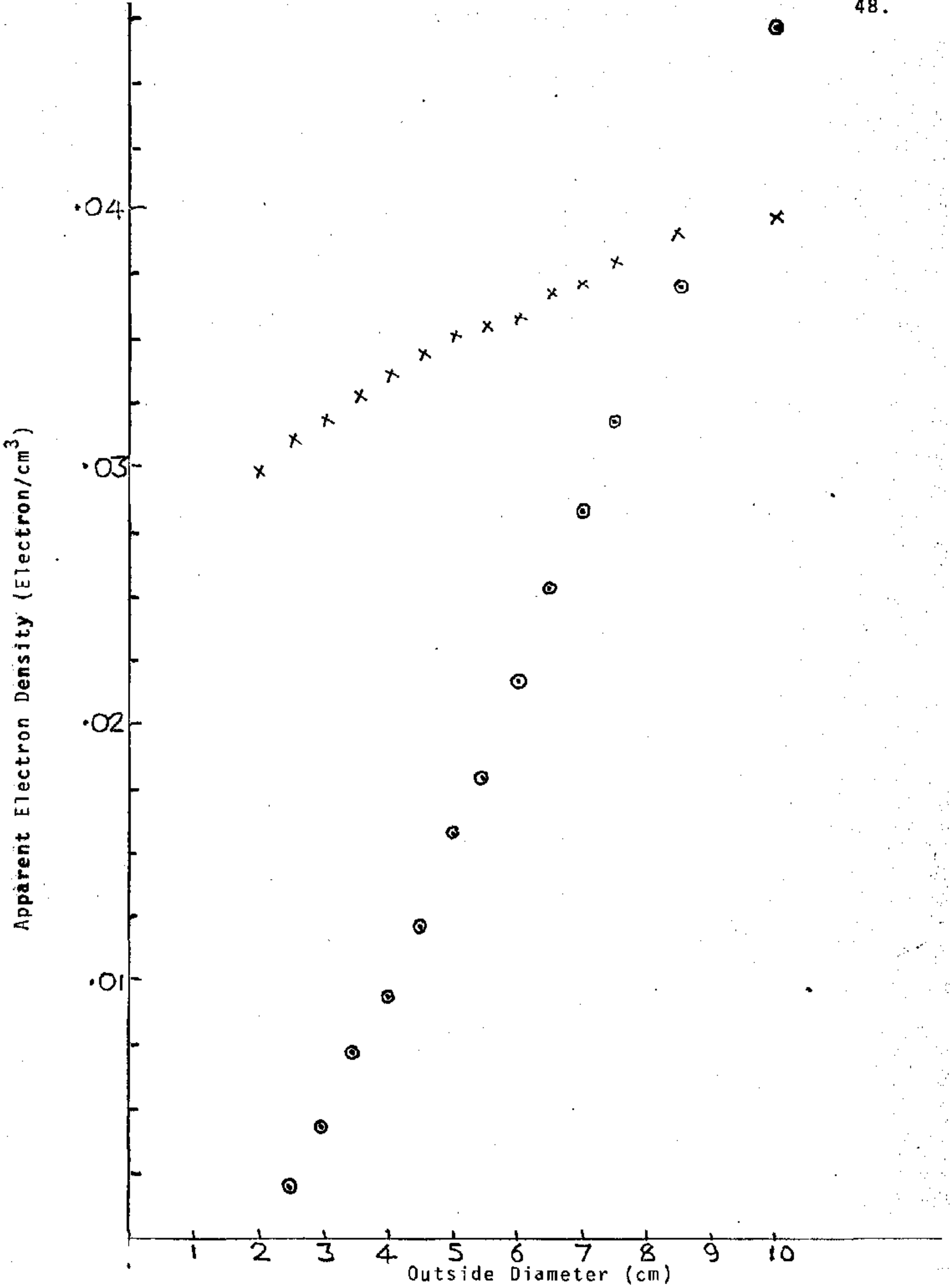

Fig.7-2: Electron Densities for Various Outside Diameters of a Lucite Rod with a 2 cm Central Hole (⊙) and without a 2cm Central Hole(x

counts for air [(S/T)air] was found to be $0.56 \pm .013 \times 10^{-4}$. For a lucite rod of 2.50cm external diameter having a central hole of 2cm diameter the ratio of the scattered to transmitted counts [(S/T) lucite-air] was found to be $1.39 \pm .04 \times 10^{-4}$. This shows that the enclosed air can offer significant contribution to the observed scattered counts while the calculations assumed that this contribution is negligible.

The experimental curves of electron densities as a function of diameter for lucite cylinders with and without the central hole of 2cm are shown in fig.7-2.

Fig.7-3 shows the predicted curves for double and single scattering for the linear attenuation coefficient $\mu = 0.165\text{cm}^{-1}$ and $\mu = 2.0\text{cm}^{-1}$. The linear attenuation coefficients of the samples considered in the present work lie in between the above μ values. (See table 7-1). The curves of double/single scattering for the various μ encountered in the present study are shown as a function of sample diameter in fig. 7-4. It is apparent from figs. 7-3 and 7-4 that although qualitatively the amount of multiple scattering will increase with increase in sample size, the quantity of multiple scattering detected may not necessarily increase with sample size. In fact the quantity that increases with object size is the ratio of the multiple scattered to the single scattered events.

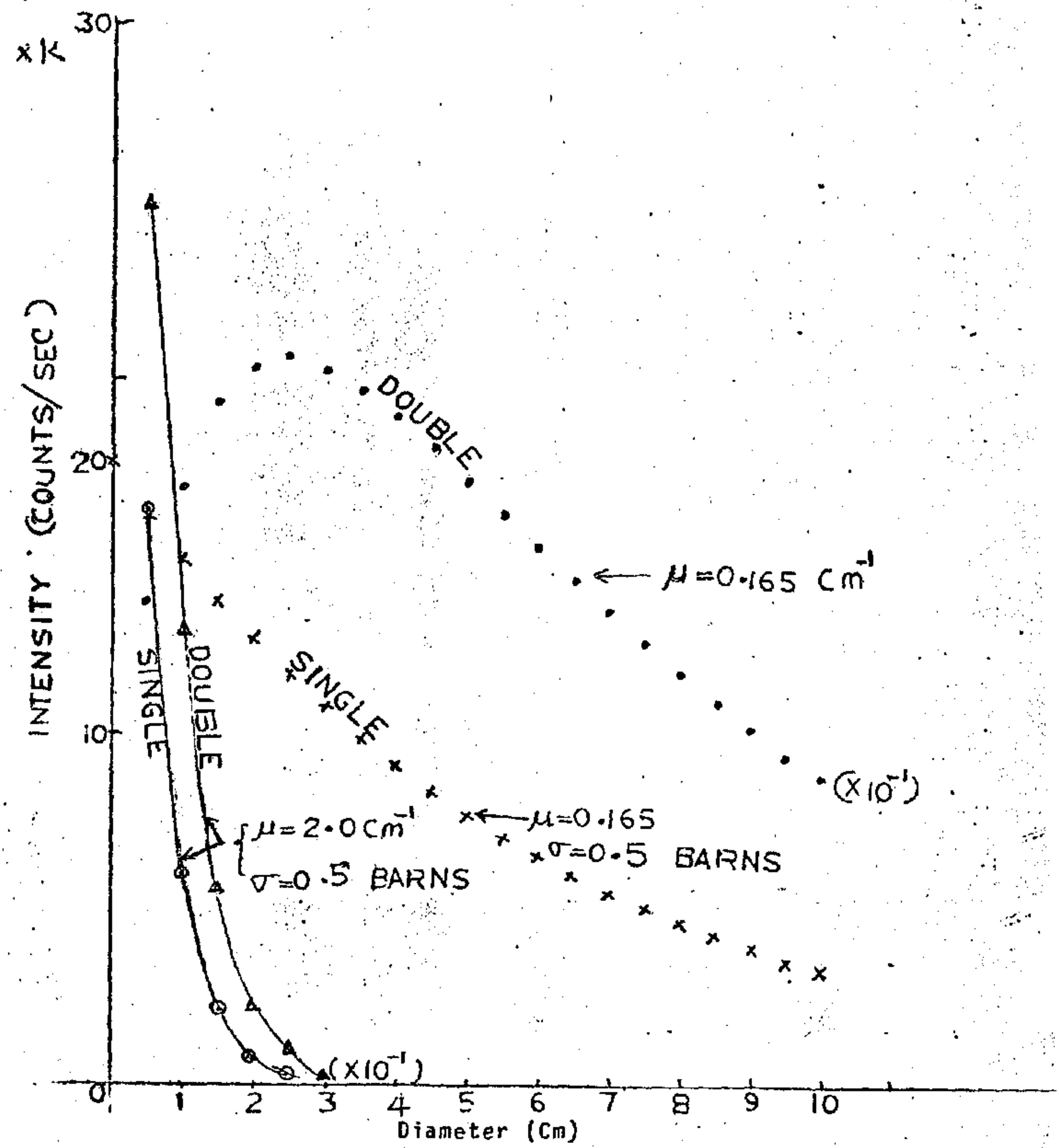

Fig.7-3: Single and Double Scattered Intensities as a Function of Lucite Diameter for μ=0.165cm^{-1} and μ=2.0cm^{-1}

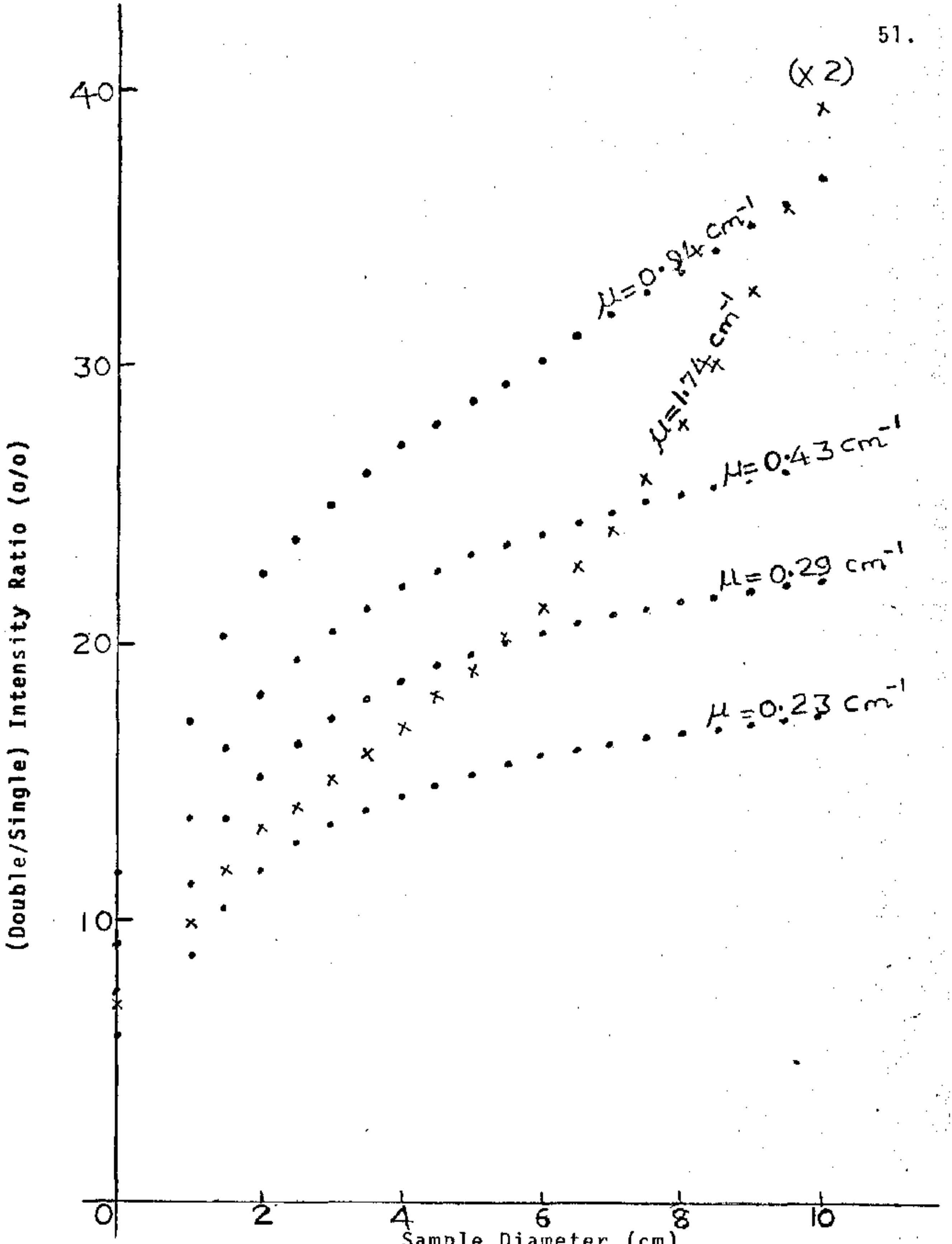

Fig.7-4: (Double/Single) Scattered Intensity Ratio as a Function of Sample Diameter for [$\mu=0.23cm^{-1}$ lucite; $\mu=0.29cm^{-1}$, Graphite; $\mu=0.43cm^{-1}$, Teflon; $\mu=0.94cm^{-1}$, Aluminum and $\mu=.74cm^{-1}$, Bone Composition (hydroxyapatite)]

2. RESULTS OF DENSITY MEASUREMENTS:

The measured densities were all calculated from equation (2-7), which makes the conventional assumption that the number of electrons per unit volume is constant [6].

Method 1: (Set A)

The results of the density measurements using the bare sample method (Set A) are shown in figs. (7-5)-(7-7) It is evident that the calculated densities are much higher than the true or Archimedes densities. The results also show that the higher the density contrast between the sample and the standard used in the measurement the greater the deviation of the Compton density from the Archimedes density. It is also apparent from these curves that the observed density for a given sample increases with increase in the diameter of the sample. If the observed density of the sample which has the same diameter as the standard is taken as a reference density, then we notice that the observed densities for similar samples, but with diameters greater than the diameter of the fixed sample will increase in value while the densities observed for similar samples but with diameters less than that of the fixed sample will decrease. This is, however, obvious since the ratio of the multiple scattered to the single scattered photons is much higher for large diameters than for small diameters (see fig.7-4). The rate of increase of the ratio of multiple scattered to single scattered photons as shown in fig. 7-4 will depend on the value of μ and hence the density of the sample.

The corrected densities for the Set A measurements are also plotted in fig. (7-8) through (7-7). The corrected densities were obtained as follows:- from the observed scattered counts for both the sample and the standard the contributions due to double scattering were extracted using the appropriate curves in fig.7-4; Equation 2-7 was then used to calculate the Compton density from the corrected scattered counts and transmission measurements.

Method 1 (Set B)

The results of the density measurements using the bare sample method (Set B) are presented in figs.(7-8) through (7-10). The observed densities like those of Set A are much higher than the Archimedes densities. However, unlike the results of Set A there is no remarkable dependence on dimensions. This may be explained by the fact that the scattered photons which have suffered more than one collision are about the same in the sample under investigation and the standard employed in the measurement. The observed discrepancy between the Compton scatter density and the Archimedes density in this set of measurements may then be attributed mainly to density and linear attenuation contrast effects

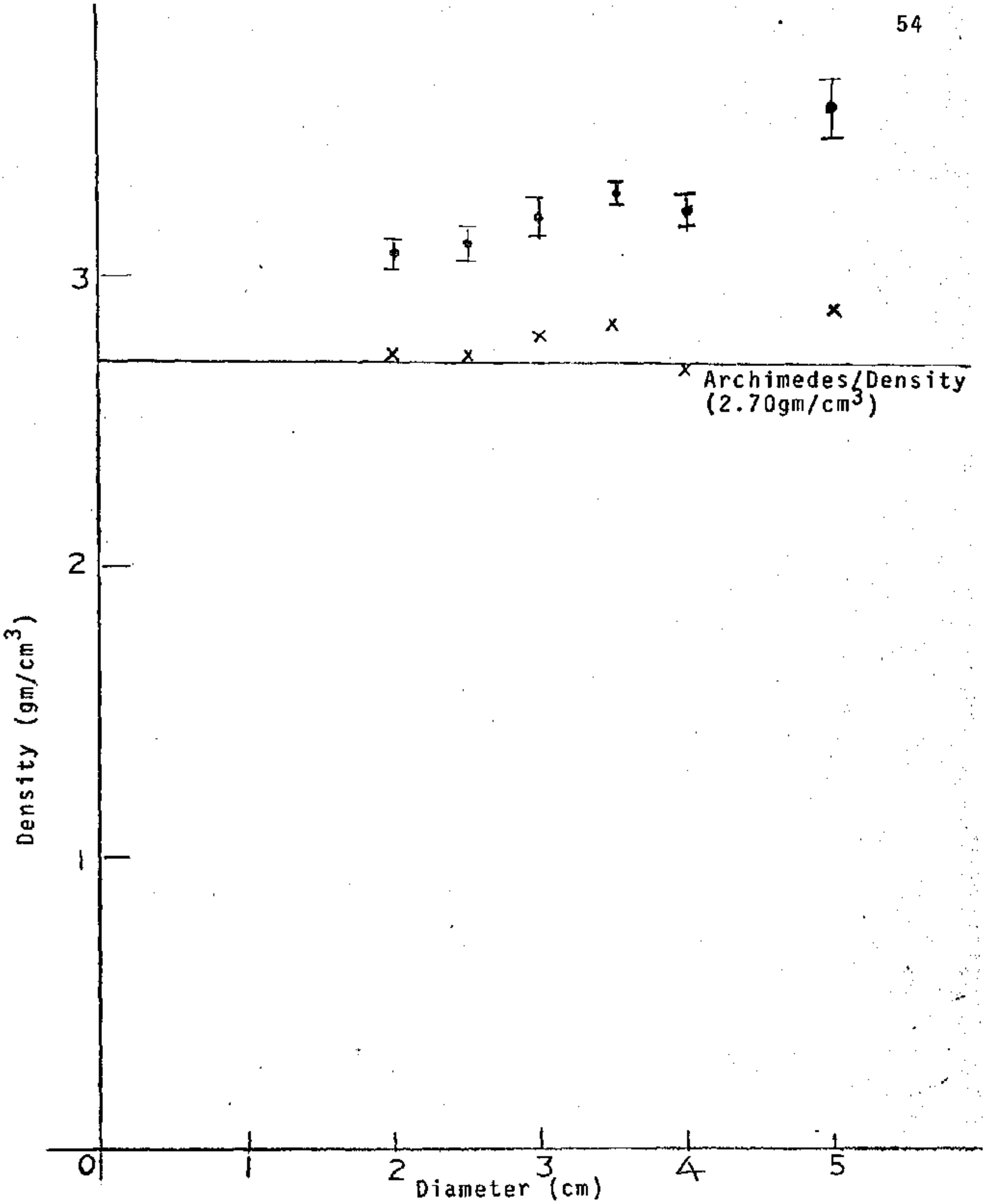

Fig.7-5: (Method 1; Measurement Set A - Using a Single Lucite Standard of Diameter 3.0cm). The observed (.) and Corrected (x) Densities of Aluminum by Compton Method and True Density (Archimedes) as a Function of Sample Diameter of Aluminum

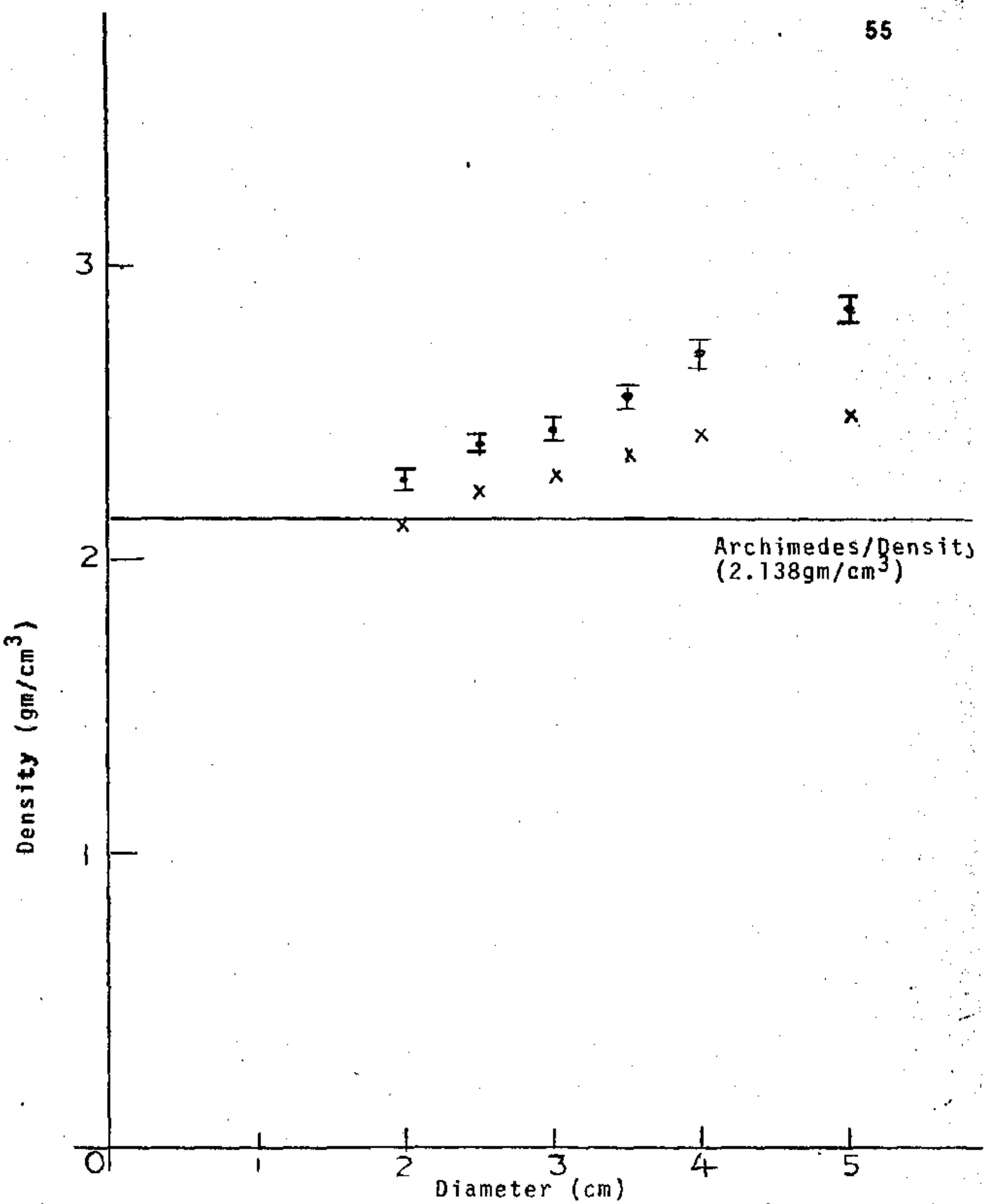

Fig.7-6: (Method 1; Measurement Set A - Using a Single Lucite Standard of Diameter 3.0cm). The Observed (.) and Corrected (x) Densities of Teflon by Compton Method and True Density (Archimedes) as a Function of Sample Diameter of Teflon

TABLE OF CONTENTS

LIST OF TABLE

LIST OF FIGURES

DEDICATED TO THE GLORY OF GOD

1 - INTRODUCTION

A knowledge of the body mineral content is of value since it is one of the physical indicators in the clinical investigation of the various disease states. The information on the body mineral content, for example, is valuable in the diagnosis of such diseases as Osteomalacia and Osteoporosis as well as in the continuing study of bone formation, development and removal processes and overall human development [10]. The mineral content of the body usually diminishes after middle age, sometimes to such an extent that the bone strength is seriously reduced. The Physician must therefore have some way of measuring the mineral content if the loss of mineral is to be controlled by diet or drugs. For non-living subjects the measurement of the mineral content is simple and straightforward. For living subjects the determination has to be done in-vivo and therefore requires special techniques.

For several years the quantitative determination of bone mineral content has constituted one of the research areas in medical physics. However, due to the complicated nature of the problem with the consequential limitations needed to uphold the safety of the patient, different versions of bone mineral content determination in vivo have emerged in the past decade.

There are at present two major clinical methods for in vivo measurement of bone mineral content. These are the Radiographic technique which makes use of an X-ray source and a standard (aluminum wedge) and Photon absorptiometry technique which uses a radioisotope and a scintillation detector.

In the Radiographic technique [11, 21, 23, 29], the exposure images of the standard wedge and the bone under investigation are obtained simultaneously on film. The X-ray attenuation through the investigated bone and the wedge are compared by means of a photodensitometer and computer. To relate the attenuation to a density the assumption is made that attenuation in the skin and flesh is small and that the bone being investigated has a known shape. Then from the volume of the bone section and the attenuation in passing through that section, it is possible to determine the relative amounts of the various constituents from knowledge of the chemical composition of the bone. Extensive research work has been carried out on this technique [29]. Precision of better than 20% is difficult to obtain with this technique and this makes it not quite satisfactory for practical use in clinics where high accuracy is desired.

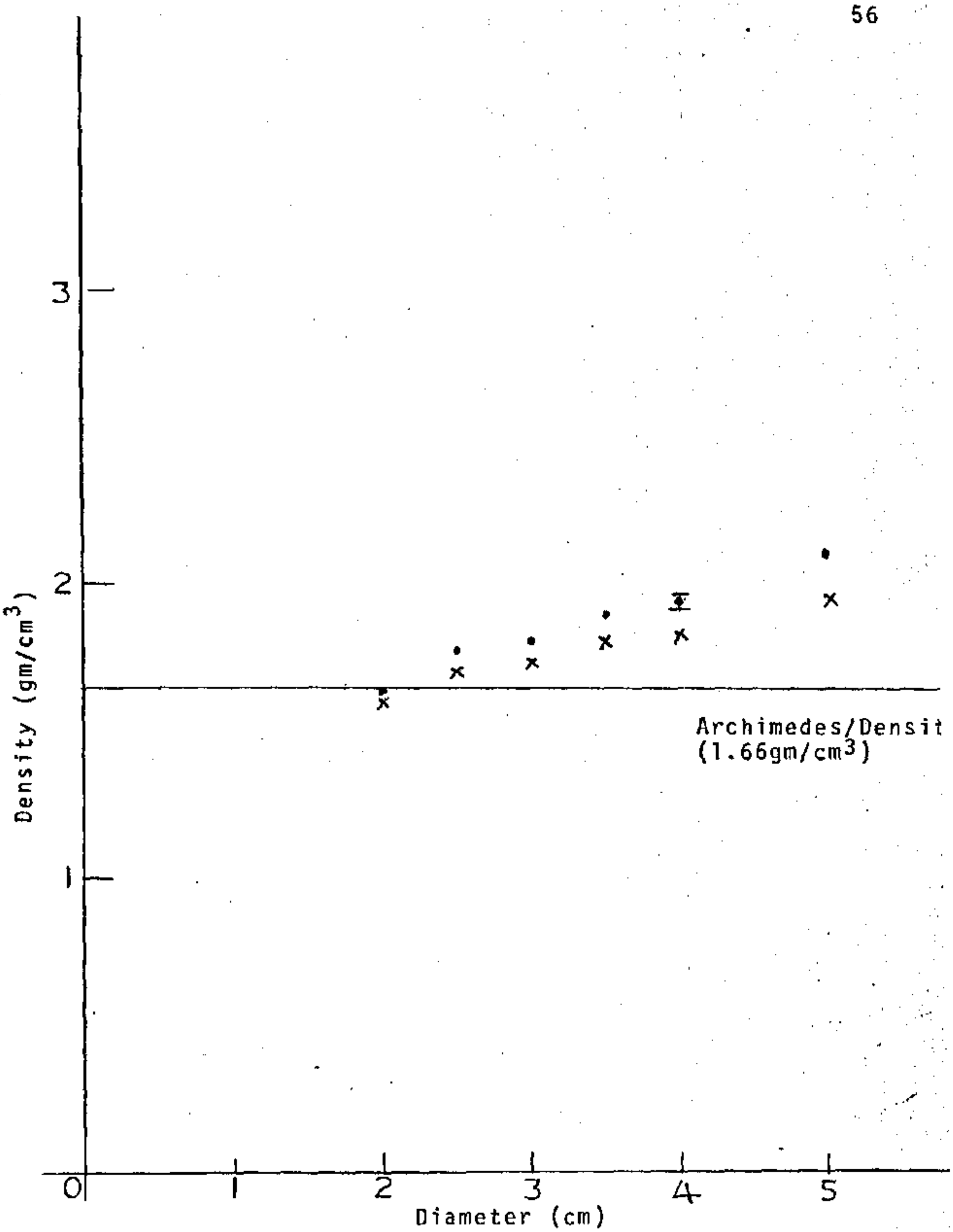

Fig.7-7: (Method 1: Measurement Set A - Using a Single Lucite Standard of Diameter 3.0cm) The Observed (.) and Corrected (x) Densities of Graphite by Compton Method and True Density (Archimedes) as a Function of Sample Diameter of Graphite

between the sample and standard.

The corrected densities for the set B measurements are plotted in figs. (7-8) through (7-10). The corrections show a reasonable amount of improvement over their initial values.

<u>METHOD 2 (Set A' and Set 13')</u>

The results of these measurements are plotted in figs. 7-11 and 7-12. The results of Set A' and Set B' are very similar to the results of Set A and Set B in Method 1 respectively.

The corrected densities for the set B' measurements using the curves in fig. (7-4) are shown in fig.(7-12). The corrections here are poor when compared to those obtained for Set B (see fig. (7-8) through (7-10). This is, however, not surprising since the curves in fig. (7-4) were not prepared for the simulation model in question. We observe that the corrections obtained for aluminum are worse than those obtained for teflon. This may be attributed to the fact that the linear attenuation contrast between aluminum and lucite ($\mu_{aL} \approx 0.8 cm^{-1}$) is higher than the linear attenuation contrast between teflon and lucite ($\mu_{tL} \approx 0.2 cm^{-1}$). In order to effectively correct for multiple scattering in the density measurements in Method 2 a different set of curves of double/single scattering which will take into account the linear attenuation coefficient of both

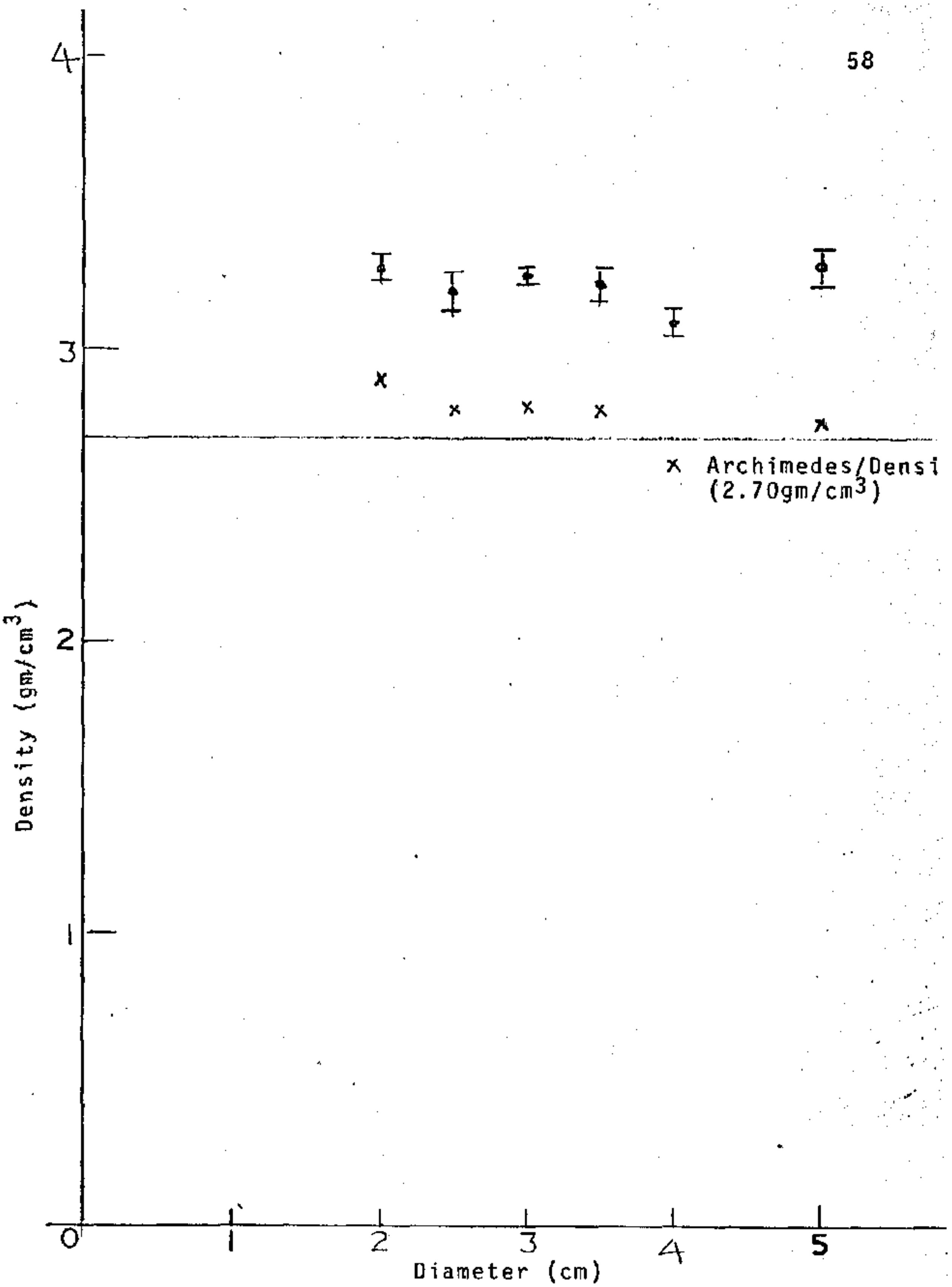

Fig.7-8: (Method 1 Measurement Set B - Using Varying Diameters of Lucite Standard). The Observed (.) and Corrected (x) Densities of Aluminum by Compton Method and True Density (Archimedes) as a Function of Sample Diameter of Aluminum

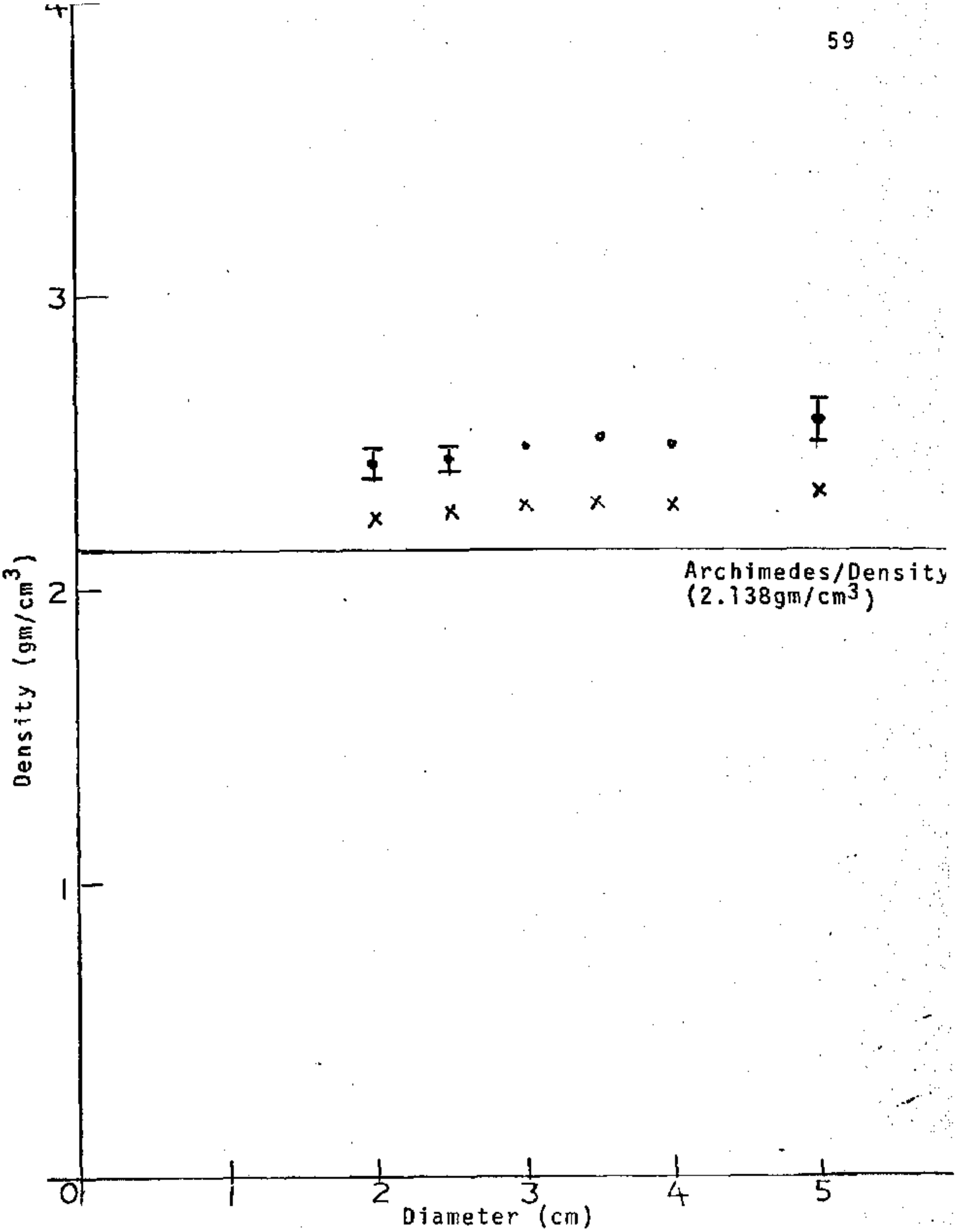

Fig.7-9: (Method 1 Measurement Set B - Using Varying Diameters of Lucite Standard) The Observed (.) and Corrected (x) Densities of Teflon by Compton Method and True Density (Archimedes) as a Function of Sample Diameter of Teflon

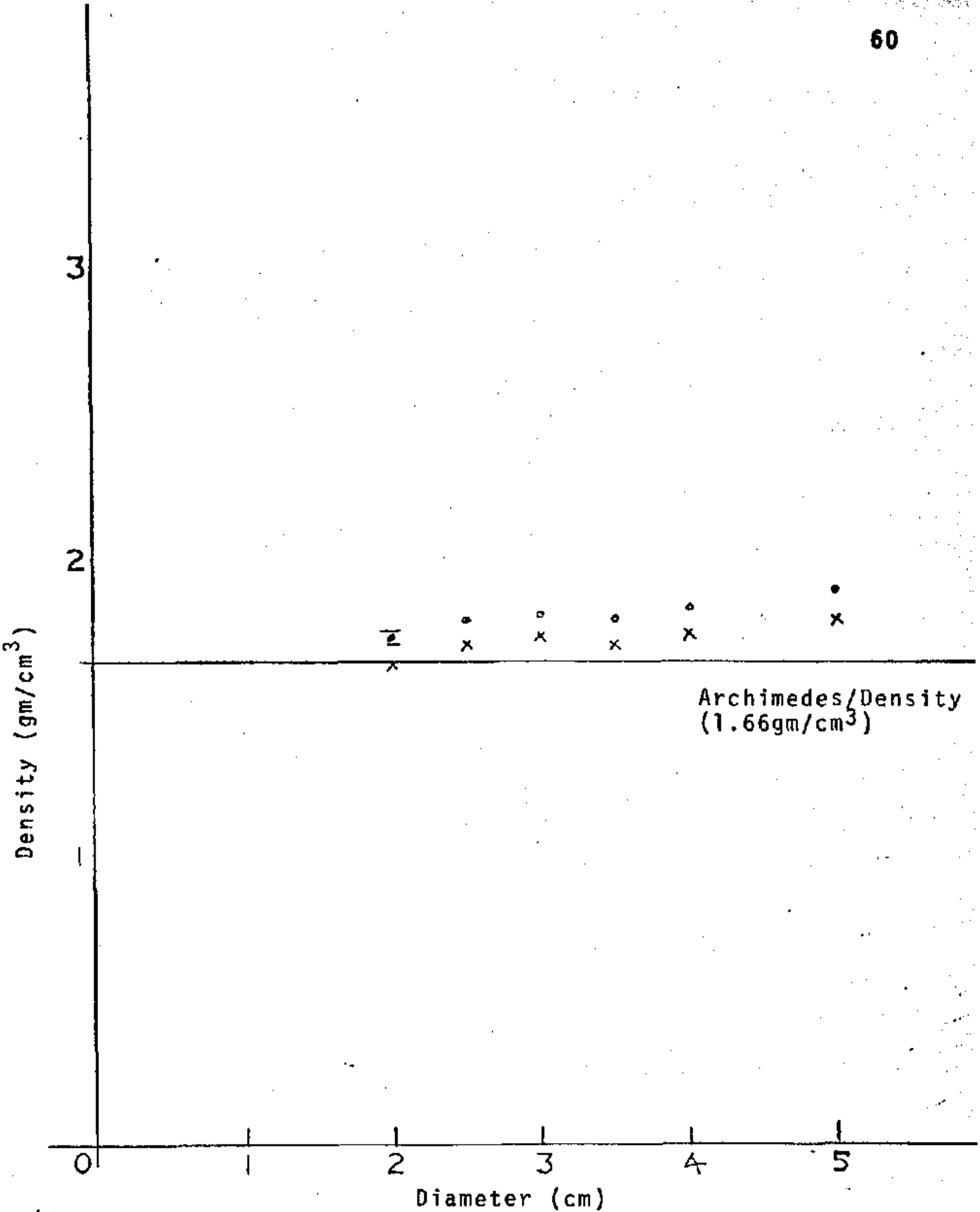

Fig.7-10 (Method 1 - Measurement Set B using Varying Diameters of Lucite Standard) The Observed (.) and Corrected (x) Densities of Graphite by Compton Method and True Density (Archimedes) as a Function of Sample Diameters of Graphite

the enclosed sample and the enclosing sample have to be produced from equation (4-8).

In fig. (7-12) we observe that the density obtained for the water sample using the Compton scatter densitometer compares very well with the Archimedes value. This is because the density contrast and the linear attenuation contrast between the water sample and lucite standard are reasonably low (see table 7-1).

It is therefore apparent that using samples and standards that have negligible density and linear attenuation contrasts would yield Compton densities that would agree excellently with the Archimedes densities. This fact can further be demonstrated by using teflon as a standard in determining the density of Aluminum by the Compton method. The results realized show reasonable improvement (about 70%) over the results obtained with lucite as standard.

The attenuation coefficient for bone in the range of energy of interest was found to be 1.74 cm^{-1} and the double/single scattering ratio is given in fig.7-4. The attenuation coefficient for tissue is about 0.24 cm^{-1} [29] and may be approximately represented in fig.7-4 by μ = 0.23 cm^{-1} which corresponds to lucite.

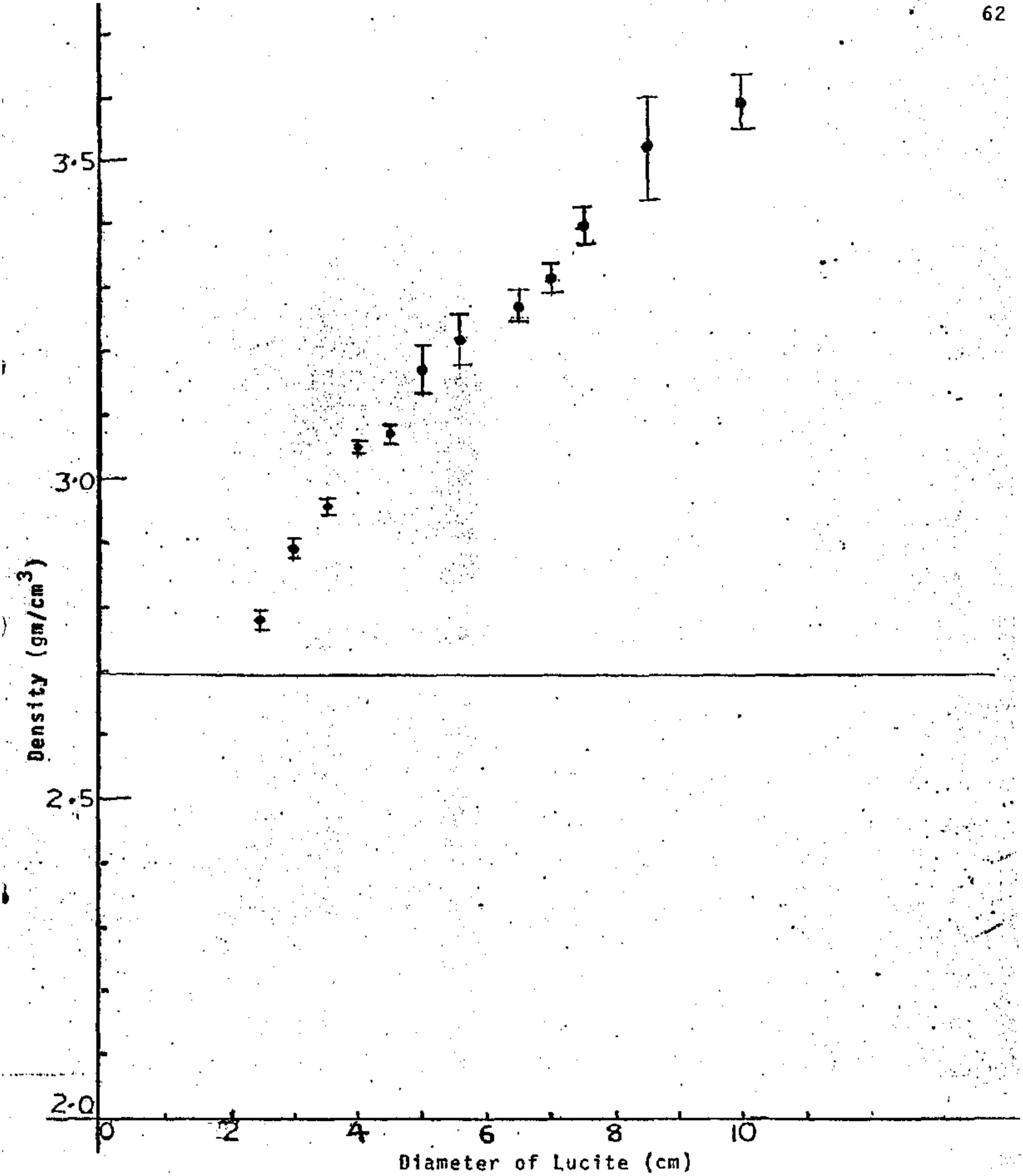

Fig.7-11: (Method 2: Measurement Set A' using a Single Lucite Standard of Diameter 4.5cm). The Observed (.) Densities of Aluminum by Compton Method and True Density (Archimedes) as a Function of Outside Diameter of Lucite

Fig.7-12: (Method 2: Measurement Set B' using Varying Diameters of Lucite Standard). The observed (.) Densities of Aluminum, Teflon, and Water; and The Corrected Densities of Aluminum (⊗) and Teflon (x) by Compton Method and True Density (Archimedes) as a Function of Outside Diameters of Lucite.

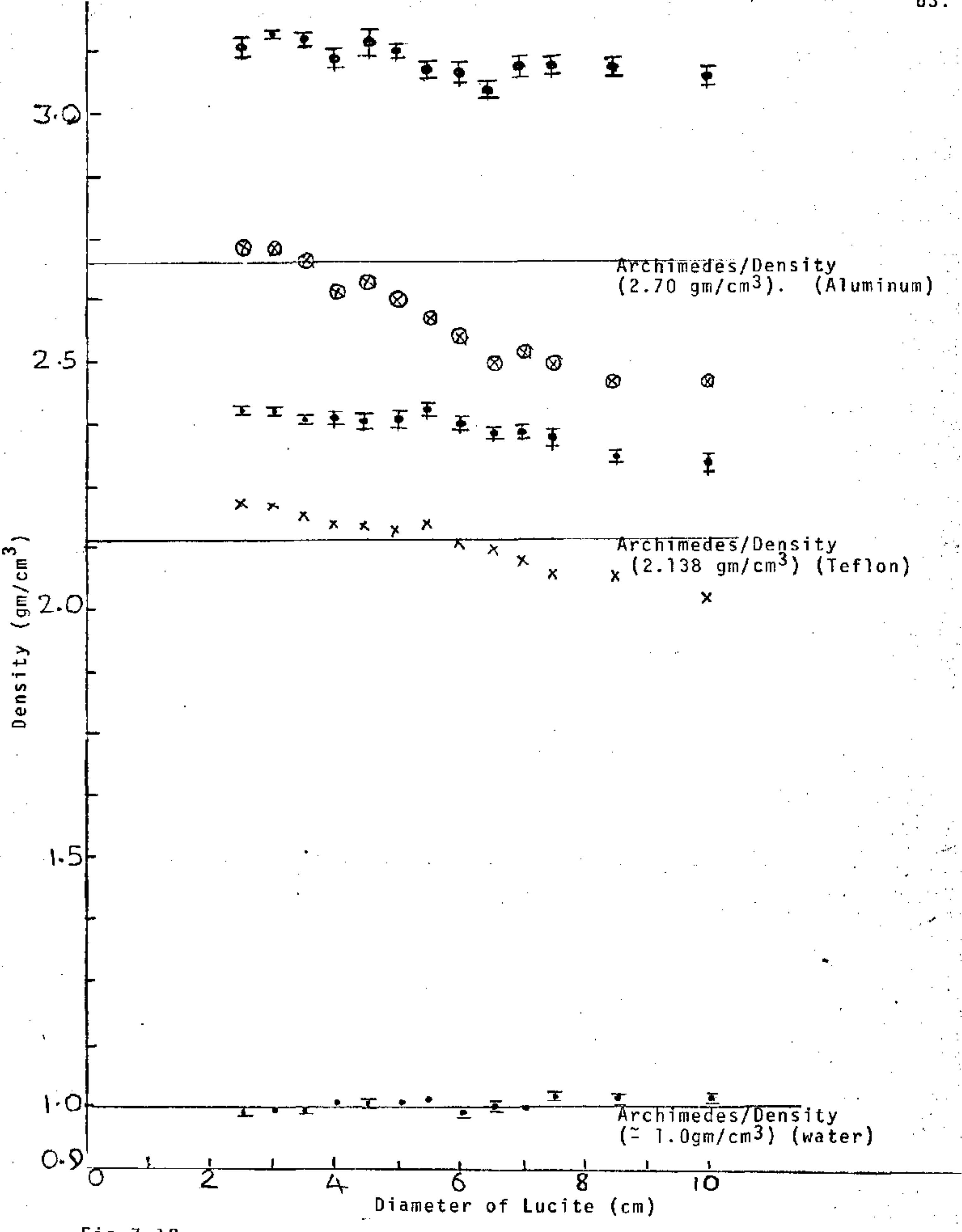
3.0
2.5
2.0
1.5
1.0
0.9
Density (gm/cm3)
Archimedes/Density
(2.70 gm/cm3). (Aluminum)
Archimedes/Density
(2.138 gm/cm3) (Teflon)
Archimedes/Density
(≃ 1.0gm/cm3) (water)
0
2
4
6
8
10
Diameter of Lucite (cm)

Fig.7-12

CONCLUSION:

It has been demonstrated that the measured electron density using the Compton scatter densitometer is influenced by the density and changes in the diameter of both the sample and the standard. It is also evident from the theoretical analysis that the influence of the linear attenuation factor becomes well pronounced for large diameters. These parameters determine the magnitude of the multiple scatter contribution collected at the nuclear counter.

It has been shown experimentally that the dependence on dimensions will be substantially reduced by using samples and standards of equal dimension. The studies also showed that the discrepancy between the Compton density and the Archimedes density will be improved if the density and linear attenuation contrast. between the sample under investigation and the standard employed are small (≤ 0.2).

A theoretical evaluation of double scattering contribution has been made and applied to some experimental data. The ultimate result show a reduction in the observed discrepancy between the Compton density and the Archimedes density by a factor of about half.

The evaluation of triple scattering for further improvement of the result is recommended. A detailed investigation of the influence of the coherent scattering cross-section in the determination of bone density using the Compton scatter densitometer is suggested.

REFERENCES

1. Bertin, E.P.; Principle and Practice of X-Ray Spectrometric Analysis; Plenum Press New York-London (1970).

2. Cameron, J.R. and Sorenson, J.A.; Science, 142, 230 (1963).

3. Cameron, J.R., Mazess, R.B. and Sorenson, J.A.; Invest. Radiol. 3, 141 (1968)

4. Cameron, J.R. and Skofronick, J.G.; Medical Physics; John Wiley & Sons Inc. (1978)

5. Charlotte, D.M. and Evans, R.D. Rev. Mod. Phys. Vol. 24 No. 2 (1952)

6. Clarke, R.L. and Van Dyk, G.; Phys. Med. Biol. Vol. 18, No.4 (1973)

7. Colbert, C., Mazess, R.B., and Schmidt, P.B.; Invest. Radiol. 5. (1970).

8. Evans, R.D.; The Atomic Nucleus, McGraw-Hill Book Company, Toronto.(1972)

9. Fitzgerald, J.J., Brownell, G.L., and Mohaney, F.J.; Mathematical Theory of Radiation Dosimetry; Gordon and Breach Science Publishers, Inc. N.Y. (1967)

10. Garrett, C.W.; Progress in Methods of Bone Mineral Measurement (1968)

11. Heuck, F.; Progress in Methods of Bone Mineral Measurement (1968)

12. Huddleston, A.L., and Bhaduri D.; Phys. Med. Biol.24 (1979)

13. Huddleston A.L., Bhaduri D., and Weaver, J.; Phys. Med. Biol. 6 (1979)

14. Isotom: Bone Density System, Dept. of Biomedical Eng., S.F.I.T. and University of Zurich - Switzerland (1979)

15. Kapoor, K.K.; Ph.D. Thesis (in progress), Carleton University

16. Way, Katherine; (Editor); Academic Press, New York and London

(a) Nuclear Data Tables, Vol. 7 No. 6 (1970)

(b) Atomic Data, Vol.5, No. 1 (1973)

17. Kennett, T.J. et al; J. Assoc. Can. Rad., 23, 168, (1972)

18. Kennett, T.J. and Webber, C.; Physics, Med.Biol.; 21, 5, 770 (1976)

19. Kuo, S.S.; Computer Applications of Numerical Methods. Addison-Wesley Publishing Company, Mc. Philippines (1972)

20. Lachmann, E., and Whelan, M , Radiology, 26, 165, (1936)

21. Mortimer, A.J.; The Measurement of Bone Mineral Content Using Scattered and Transmitted X-rays; M.Sc. Thesis, Carleton University, (1974)

22. Olkkonen, H., et al; "Measurement of Bone Mineral Density Using Coherent and Compton Scattering; Int. Conference on Bone Mineral Measurement; New Orleans, Jan.26-28, (1976)

23. Rockoff, S.D.; Progress in Development of Methods in Bone Densitometry (1965)

24. Strandjord, N.M.; Inter. Conf. on Bone Mineral Measurement. (1965)

25. Stroud, A.H.; Approximate Calculation of Multiple Integrals; Prentice-Hall Inc., Englewood Cliffs, N.J. (1971)

26. Trench, F.W. and Kolman, B.; Multivariable Calculus with Linear Algebra and Series; Academic Press, N.Y. and London. (1972)

27. Webber, C.E. and Kenneth, T.J.; Phys. Med. Biol. 21, 5, 760, (1976)

28. White, D.R.; Phys. Med. Biol. 1977, 22, 2, (1977)

29. White, M.W. A Study of Bone Density Measurement Using the Photon Scattering Technique; M.Sc. Thesis, Carleton University, 1974.

30. Jaklevic, J.M.; Goulding, F.S.; "X-Ray Spectrometry" Edited by Hergiotz M.K.; Birks, L.S. Marcel Dekker, Inc. New York and Basel